AI-Driven Complexity Reduction and Multi-Physics Digital Twins

From Theory to Engineering Implementation in Nuclear Reactors

Helin Gong

Paris Elite Institute of Technology, Shanghai Jiao Tong University

Based on a series of joint works with collaborators and students in reduced-order modeling, data assimilation, and nuclear reactor digital twins

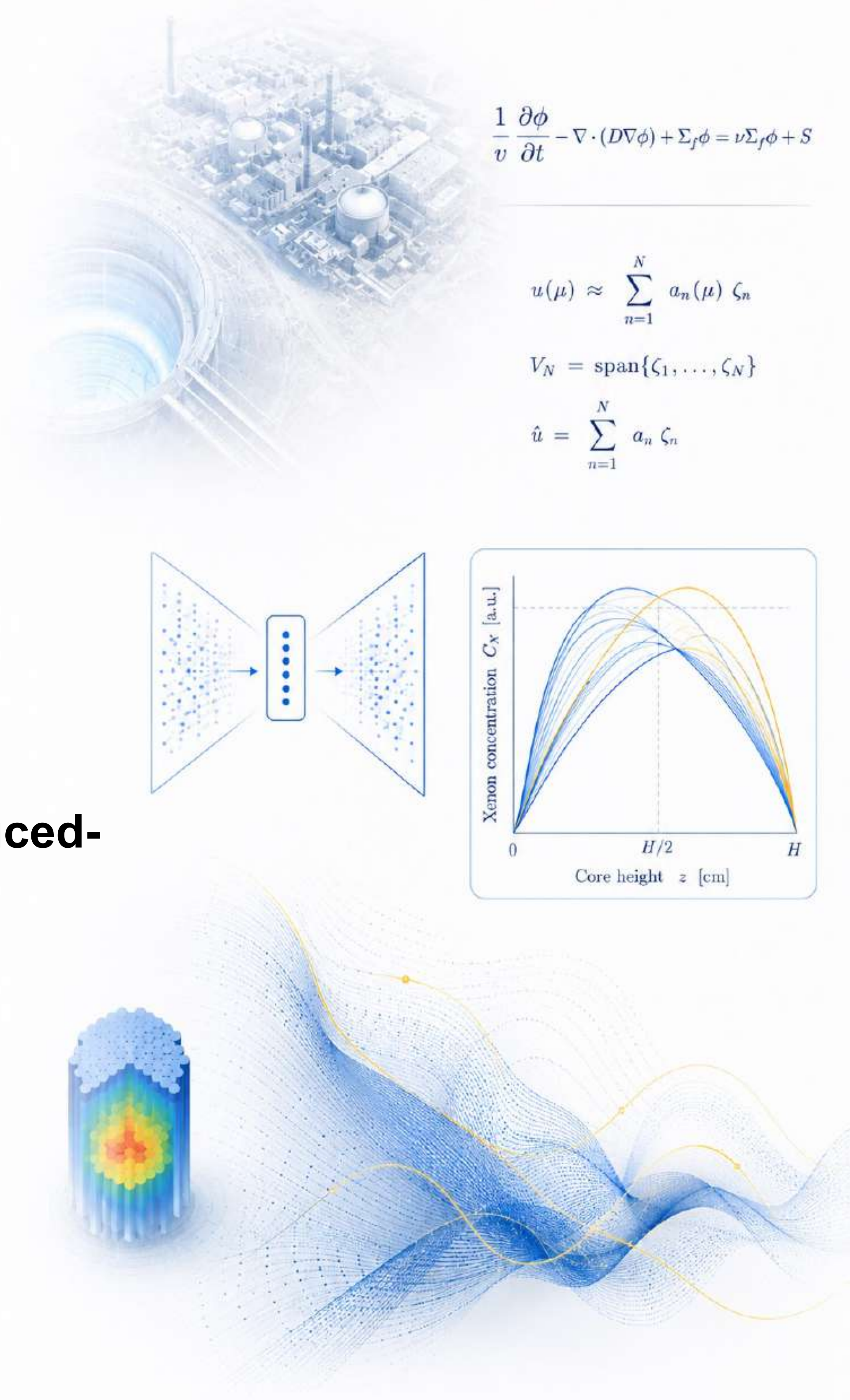

Yvon Maday's Symposium:
Mathematical and Applied Aspects of Complexity Reduction Methods

Collège de France, Paris, 22–24 June 2026

Information, uncertainty, and margin

Better reactor-state information reduces uncertainty and supports safer operational margin release

Engineering motivation		Mathematical structure			Operational consequence	
Best-estimate plus uncertainty	Governing equations	Sparse observations	**Reduced inference**	Multi-field estimation	Uncertainty reduction	**Margin support**

Sources of complexity in nuclear digital twins

Finite information
01 $\mathcal{Y}_{\mathrm{obs}}$

Noisy-measurement stability
02 $\epsilon_{\mathrm{noise}}$

Model discrepancy and parameter uncertainty
03 $\delta_{\mathrm{model}}, \mathbf{B}, \mathbf{R}$

Nonlinear solution geometry
04 $\mathcal{M}_{\mathrm{ROM}}$

Multi-field inference and trajectory forecasting
05 $\partial_t \mathcal{U}_{\mathrm{multi}}$

Engineering robustness and lifecycle
06 Λ_{safe}

How can finite, noisy, and partial information be converted into credible online safety-margin knowledge?

BEPU turns safety assessment into uncertainty-aware prediction

The key question is how much uncertainty remains in the safety margin

- Traditional conservative margins often cover model error, parameter error, and observation error.
- BEPU writes safety assessment as a prediction problem under uncertainty.

$$P_{\mathrm{top}}(t) = \int_{H/2}^{H} \int_{\Omega_{xy}(z)} P(x, y, z, t)\, dx\, dy\, dz$$

$$P_{\mathrm{bot}}(t) = \int_{0}^{H/2} \int_{\Omega_{xy}(z)} P(x, y, z, t)\, dx\, dy\, dz$$

$$\Delta I(t) = 100 \frac{P_{\mathrm{top}}(t) - P_{\mathrm{bot}}(t)}{P_{\mathrm{top}}(t) + P_{\mathrm{bot}}(t)}$$

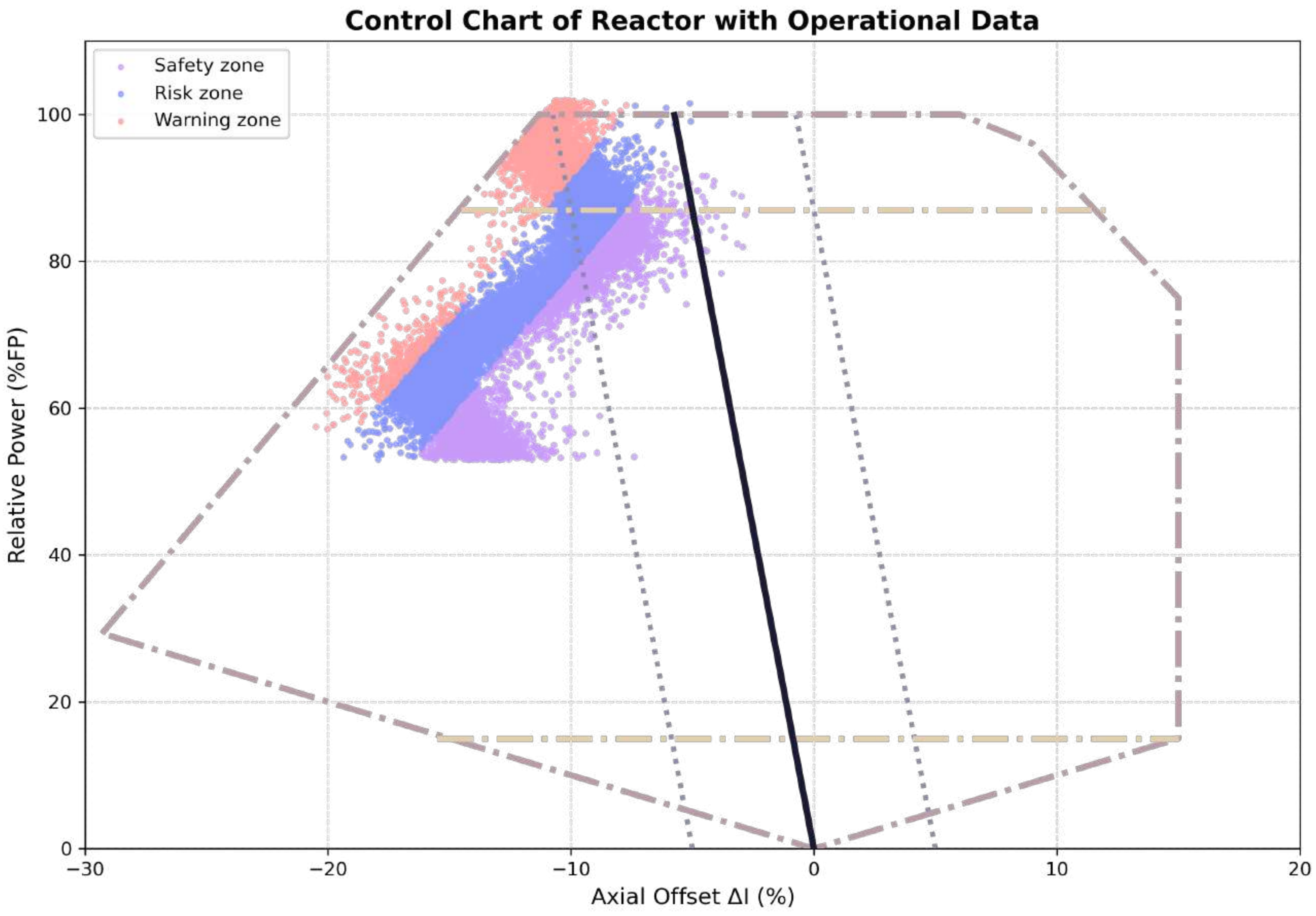

Remark: BEPU requires safety margins to be evaluated under model, parameter, and measurement uncertainty..

Lower uncertainty can release operational margin without relaxing safety

More accurate multi-physics state and safety-parameter estimation reduces unnecessary conservatism

- Reactor operation must remain safe while avoiding unnecessary loss of operating room.
- More accurate state and safety-parameter estimation reduces uncertainty and supports finer operating decisions.

Power peaking factor

$$F_Q := \frac{\max_{r\in\Omega} u(r)}{\frac{1}{V}\int_\Omega u(r)dr}$$

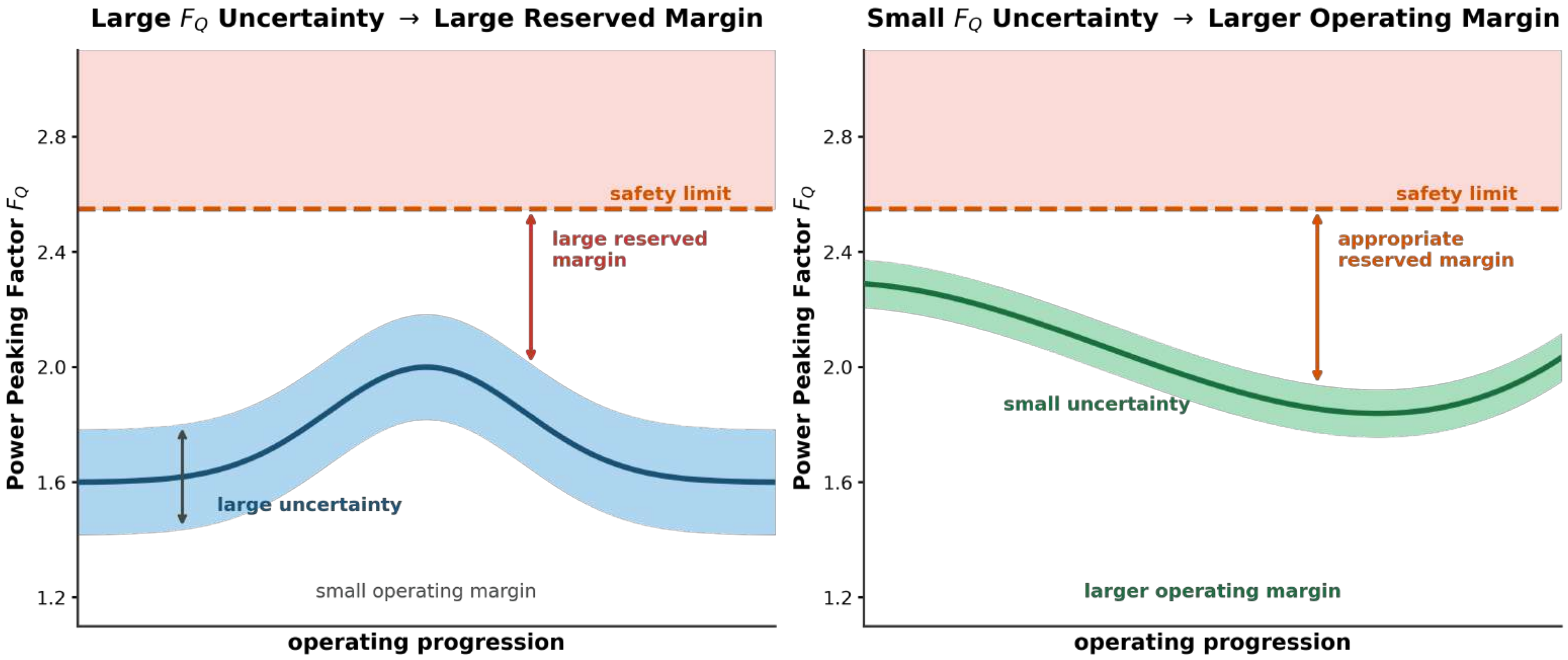

Remark: Lower uncertainty can release operational margin without relaxing safety.

The digital twin begins with a high-fidelity multi-physics control equation

Governing physics, sparse observations, and margin probability define the inference problem

Governing equation $$\mathcal{F}(u,\boldsymbol{\mu})=0,$$

State in function space $$u(\boldsymbol{\mu},t)\in\mathcal{H}$$

Sparse observation $$y_i=\ell_i(u)+e_i$$

Margin probability $$P(M(u,\boldsymbol{\mu},t)>0|\boldsymbol{y})$$

$\boldsymbol{\mu}$ operating / physical parameters

u multi-physics reactor state

ℓ_i observation functionals

e_i measurement noise

M safety-margin functional

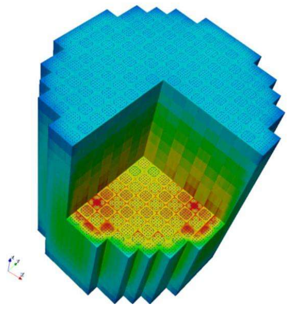

$$\frac{1}{v(E)}\frac{\partial}{\partial t}\psi(\vec{r},E,\vec{\Omega},t)+\vec{\Omega}\cdot\nabla\psi(\vec{r},E,\vec{\Omega},t)+\Sigma_t(\vec{r},E,t)\psi(\vec{r},E,\vec{\Omega},t) = \int dE'\int d\vec{\Omega}'\,[\left(\frac{\chi[E]}{k_{\text{eff}}}\right)\nu\Sigma_f(\vec{r},E',t)+\Sigma_s(\vec{r},\vec{\Omega}'\to\vec{\Omega},E'\to E,t)]\psi(\vec{r},E',\vec{\Omega}',t)$$

$$\rho c_p(T)\frac{\partial T(\vec{r},t)}{\partial t}= \nabla\cdot k(T)\nabla T(\vec{r},t)+\dot{q}(\vec{r},t)$$

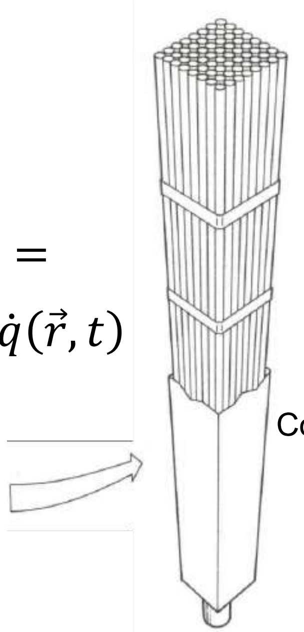

$$\rho\left(\frac{\partial\vec{v}(\vec{r},t)}{\partial t}+\vec{v}(\vec{r},t)\cdot\nabla\vec{v}(\vec{r},t)\right)=-\nabla p(\vec{r},t)+\mu\nabla^2\vec{v}(\vec{r},t)+\vec{f}(\vec{r},t)$$

Remark: Here, a nuclear reactor digital twin is an observation-conditioned inference problem built on governing physics.

High-fidelity physics stays offline; efficient inference goes online

Complexity reduction transfers physical fidelity into operational time scales

offline high-fidelity physics

multi-physics solver · slow but physically credible

$$\mathcal{F}(u,\boldsymbol{\mu}) = 0$$

multi-physics snapshots
minutes · hours · many cores

offline

reduced representation

offline database · reduced basis · low-dimensional coordinates

$$V_n = \mathrm{span}\{\varphi_1, \dots, \varphi_n\}$$
$$u \approx u_n = \textstyle\sum_{i=1}^{n} \alpha_i \varphi_i$$

offline knowledge becomes online coordinates

online

online inference

fast state reconstruction · parameter update · decision support

$$y_i = \ell_i(u(\boldsymbol{\mu},t)) + e_i$$
$$P(M(u,\boldsymbol{\mu},t) > 0 \mid \boldsymbol{y})$$

state estimate → parameter update → margin support
seconds · sub-seconds · many queries

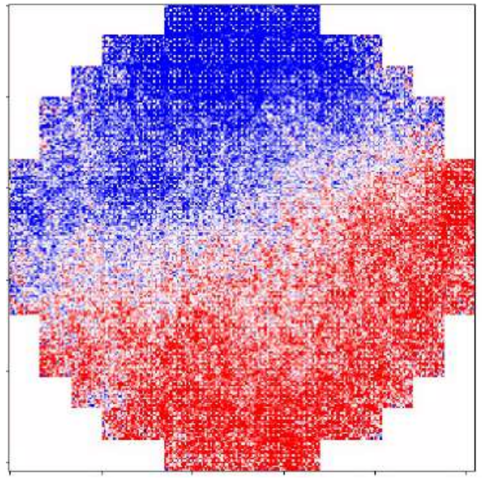

e.g. pin power distribution by
CORCA-3D, NPIC, China

High-fidelity physics is learned offline and used online through reduced coordinates.

T_{FOM} ≫ T_{Decision} ≫ T_{ROM}

hours	minutes	seconds	sub-seconds
full-order simulation	offline database	reduced inference	decision support

online decision window

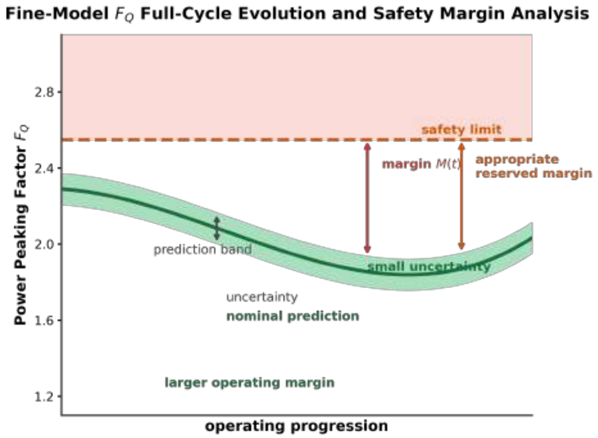

Remark: Reduced inference transfers offline physical fidelity into online operational time scales.

Sources of reactor-core complexity in reduced inference

Each bottleneck enlarges uncertainty in safety margins; each following method reduces one part of it

Model deviation

$$\mathcal{F}_{\mathrm{ROM}}(u,\mu)+\delta_{\mathrm{model}}=0$$

Observation noise

$$y_i=\ell_i(u(\mu,t))+\varepsilon_i,\qquad \mu\sim\pi(\mu)\to\pi(\mu\mid y)$$

Parameter posterior

$$P(M(u,\mu,t)>0\mid y)$$

Core reduced-inference relations

$m\ll\dim(\mathcal{H})$

Finite information

GEIM / RB

Argaud et al., JCP, 2018; Gong et al., NED, 2021

$y_i=\ell_i(u)+\varepsilon_i$

Noisy-measurement stability

CS-GEIM / regularized RB

Argaud et al., ICOSAHOM, 2017; Gong et al., NED, 2021

$\delta_{\mathrm{model}},\quad \mu\sim\pi(\mu)$

Model discrepancy and parameter uncertainty

PBDW-inspired correction / Ensemble Bayesian inference

Maday et al., IJNME, 2015; Zeng et al. (Gong), NST, 2023

$u\notin V_n$ for small n

Nonlinear solution geometry

SVD-AE / latent assimilation

Gong et al., ANE, 2022

$u=(\phi,T,X,\ldots),\quad u(t)\leftarrow u(t_0:t)$

Multi-field inference and trajectory forecasting

SHPNet / ST-GEIM / xenon dynamics

Xu et al., EAAI, 2025; Bao et al., JCP, 2025; Gong et al., NSE, 2026

$\varepsilon_i(t),\quad \text{missing data},\quad \text{drift}$

Engineering robustness and lifecycle

NN-EIM / online basis update

Li et al., CiCP, 2026; Zhang et al., NMTMA, 2025

Remark: The following methods form an uncertainty-control pipeline from finite observations to margin-informed operation.

PART I

Finite-information recovery in reduced spaces

Safety-relevant reactor fields are not fully observable

Limited sensors create the first inverse problem in reactor-core digital twins

hidden full reactor field

u

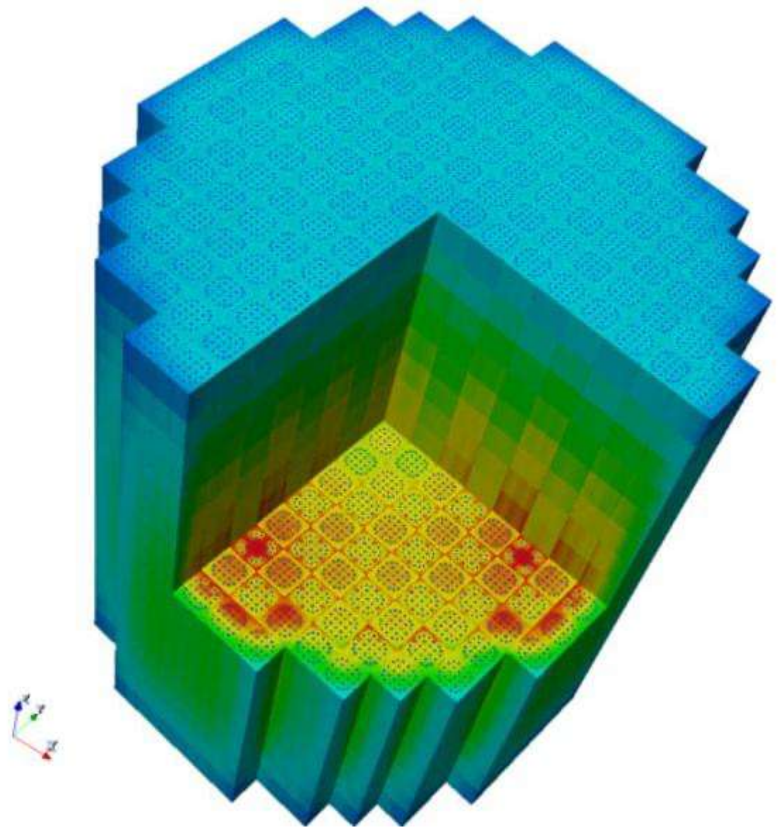

Example of HPR1000 power distribution

forward observation

$u \rightarrow \boldsymbol{y}$

$\boxed{\dim(\boldsymbol{u}) \gg \dim(\boldsymbol{y})}$

inverse reconstruction

$u \leftarrow \boldsymbol{y}$

available sparse observations

$y_i = \ell_i(u(\boldsymbol{\mu},t)) + e_i$

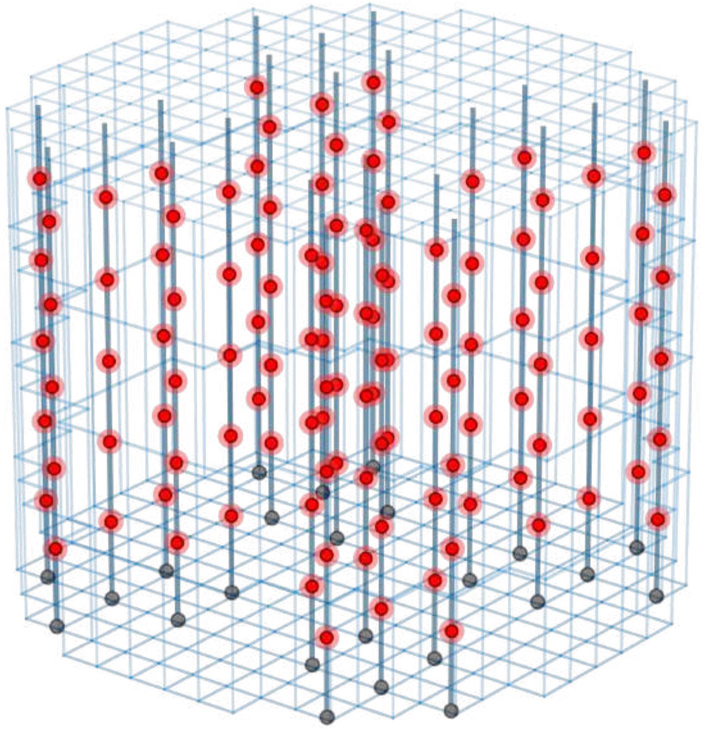

Example of HPR1000 in-core sensors

u is hidden, $y_i = \ell_i(u(\boldsymbol{\mu},t)) + e_i$ is available

Safety margins depend on full-field structure, while plant instrumentation only provides limited local measurements.

Remark: Sparse sensors create the first inverse problem: recovering safety-relevant fields from limited information.

GEIM turns sparse measurements into structured information

Observation functionals and greedy selection identify where the reduced space still lacks information

Algorithm 1: Generalized Empirical Interpolation Method (GEIM)

Input : Snapshot manifold $\mathcal{F} \subset \mathcal{V}$, Sensor dictionary Σ, Tolerance ε

Output : Reduced basis $\{q_1, \dots, q_N\}$, Selected sensors $\{\ell_1, \dots, \ell_N\}$

1 : Initialization ($n = 1$):

$$\varphi_1 = \arg\max_{\varphi \in \mathcal{F}} \|\varphi\|_{\mathcal{V}}$$

$$\ell_1 = \arg\max_{\ell \in \Sigma} |\ell(\varphi_1)|$$

$$q_1 = \varphi_1 \,/\, \ell_1(\varphi_1)$$

2 : **for** $n = 2, 3, \dots, N_{\max}$ **do**

// Step 2.1: Greedy selection of the worst-approximated snapshot

$$\varphi_n = \arg\max_{\varphi \in \mathcal{F}} \|\varphi - \mathcal{J}_{n-1}[\varphi]\|_{\mathcal{V}}$$

if $\|\varphi_n - \mathcal{J}_{n-1}[\varphi_n]\|_{\mathcal{V}} < \varepsilon$ **then break**

// Step 2.2: Greedy selection of the sensor maximizing the residual

$$\ell_n = \arg\max_{\ell \in \Sigma} |\ell(\varphi_n - \mathcal{J}_{n-1}[\varphi_n])|$$

// Step 2.3: Construct and normalize the new basis function

$$q_n = \frac{\varphi_n - \mathcal{J}_{n-1}[\varphi_n]}{\ell_n(\varphi_n - \mathcal{J}_{n-1}[\varphi_n])}$$

3 : **end for**

$$\mathcal{J}_{n-1}[\varphi] := \sum_{j=1}^{n-1} \alpha_j q_j$$

$$\text{s.t. } \ell_i(\mathcal{J}_{n-1}[\varphi]) = \ell_i(\varphi)$$

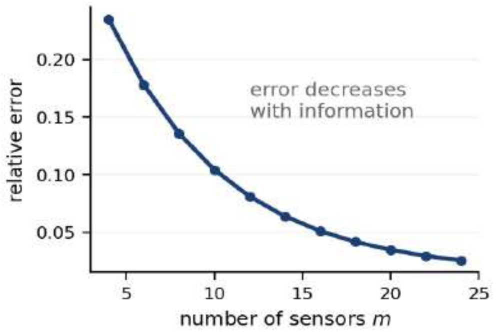

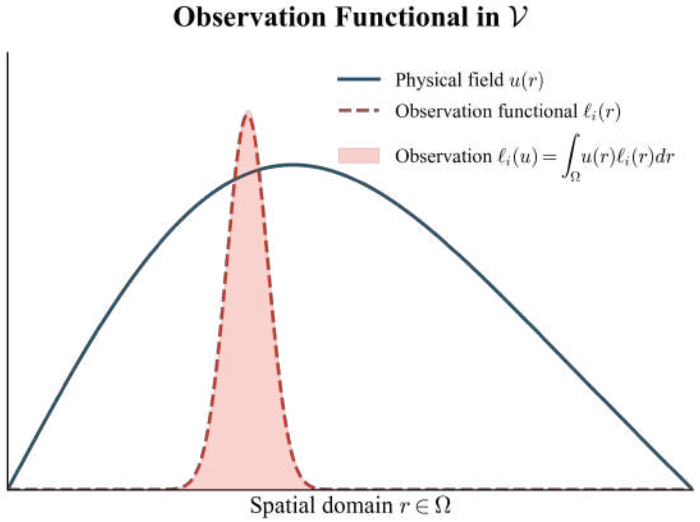

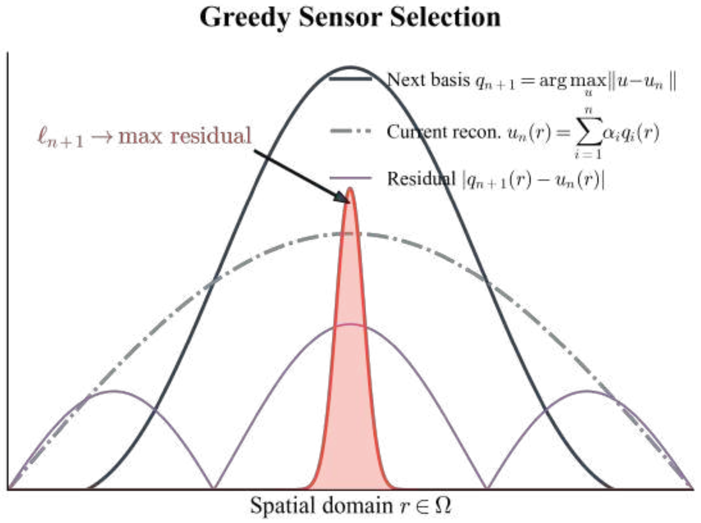

Maday & Mula, Springer, 2013; Argaud et al., JCP, 2018

Each sensor acts on u through a functional ℓ_i.
The next sensor is chosen where the current reduced space still lacks information.

Reduced coordinates connect sparse sensing with reactor-field reconstruction

Sensor observations estimate a few basis coefficients in a physics-informed reduced space

$$\boxed{\dim(u) \gg \dim(\boldsymbol{y}) > \dim(u_n)}$$

$$V_n = \mathrm{span}\{q_1, \dots, q_n\}$$
$$u(\boldsymbol{\mu}, t) \approx u_n = \sum_{i=1}^{n} \alpha_i(\boldsymbol{\mu}, t) q_i$$
$$y_i = \ell_i(u(\boldsymbol{\mu}, t)) + e_i \approx \ell_i(u_n)$$

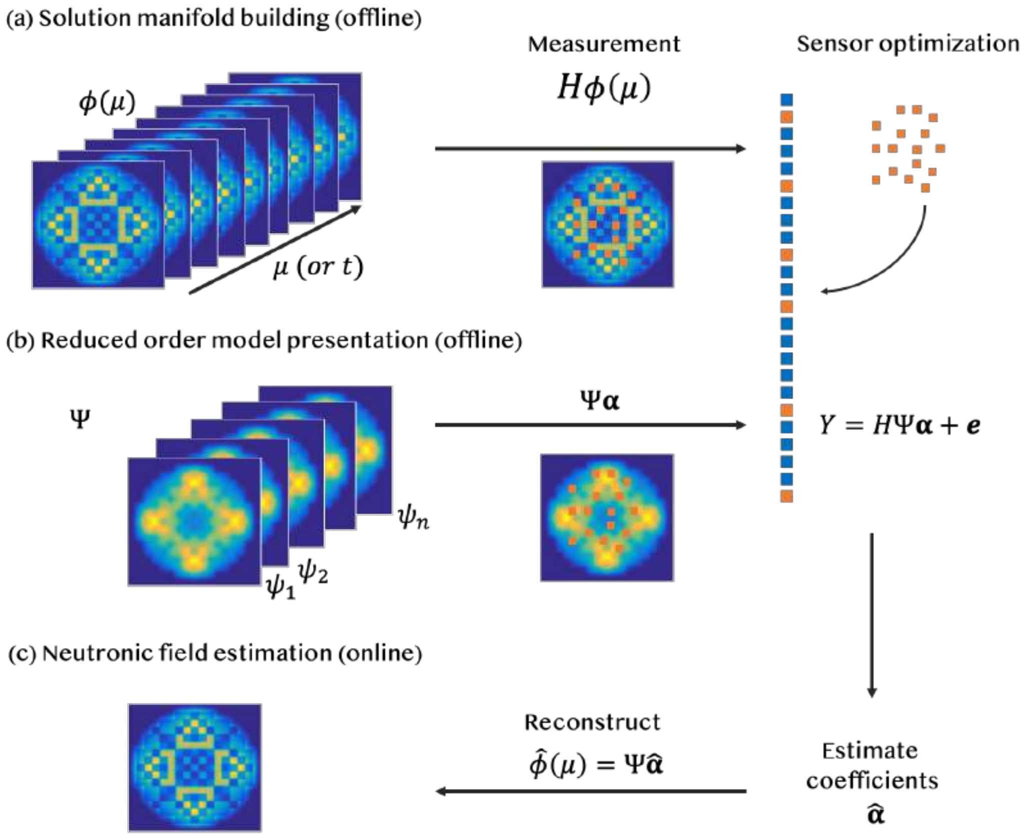

Offline-Online framework. [Gong et al., NED 2021]

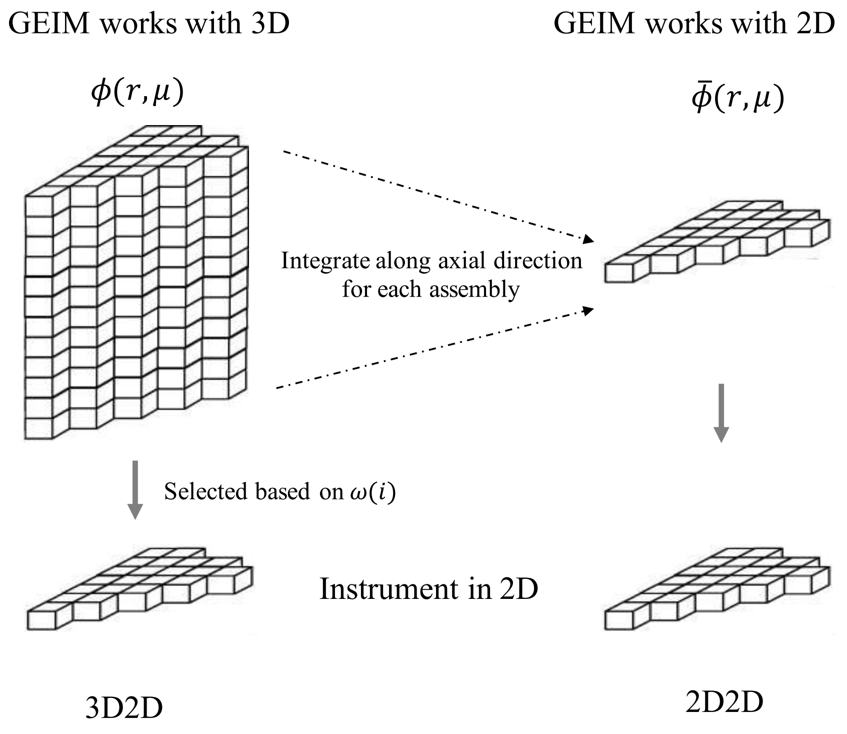

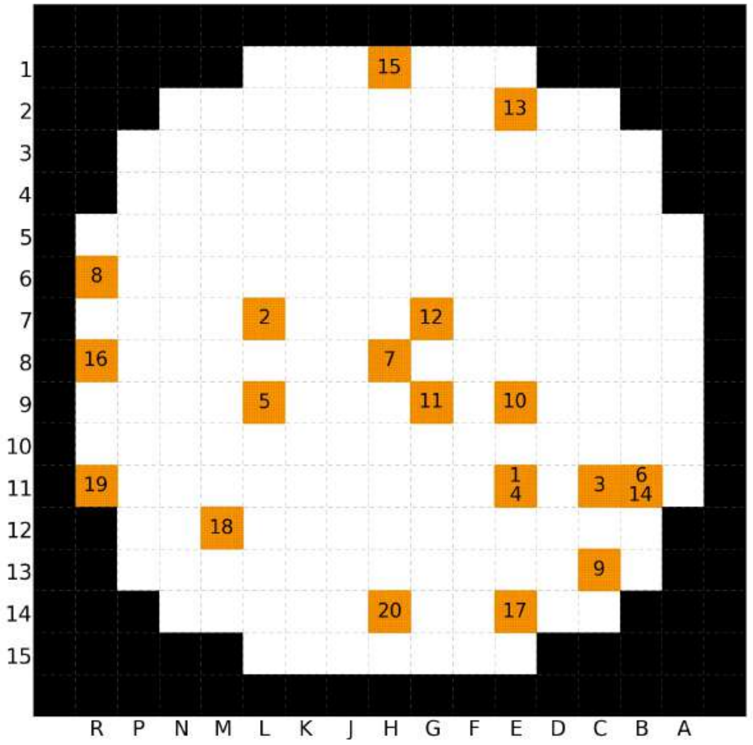

Sensor optimization of PWR1300 at EDF. [Argaud et al., JCP, 2018]

Accurate field reconstruction improves safety-parameter estimation

Reduced dimension, observation redundancy, and sensor placement jointly determine reconstruction accuracy

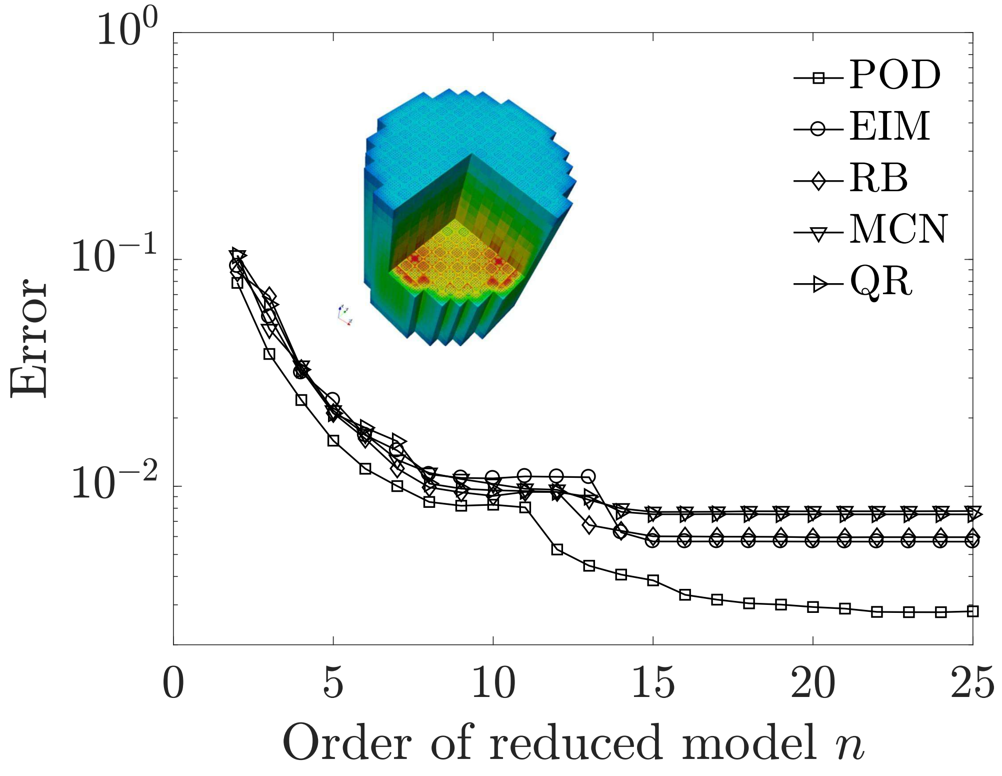

POD = Proper Orthogonal Decomposition;
EIM = Empirical Interpolation Method;
RB = Reduced Basis ;
MCN = Minimum Condition Number;
QR = QR with column pivoting

Error decreases and stabilizes as the reduced dimension *n* increases.

More observations per mode reduce the reconstruction error.

MMN = Minimum Matrix Norm;
MCN = Minimum Condition Number;
ODEIM = Oversampled EIM;
EIM = Empirical Interpolation Method

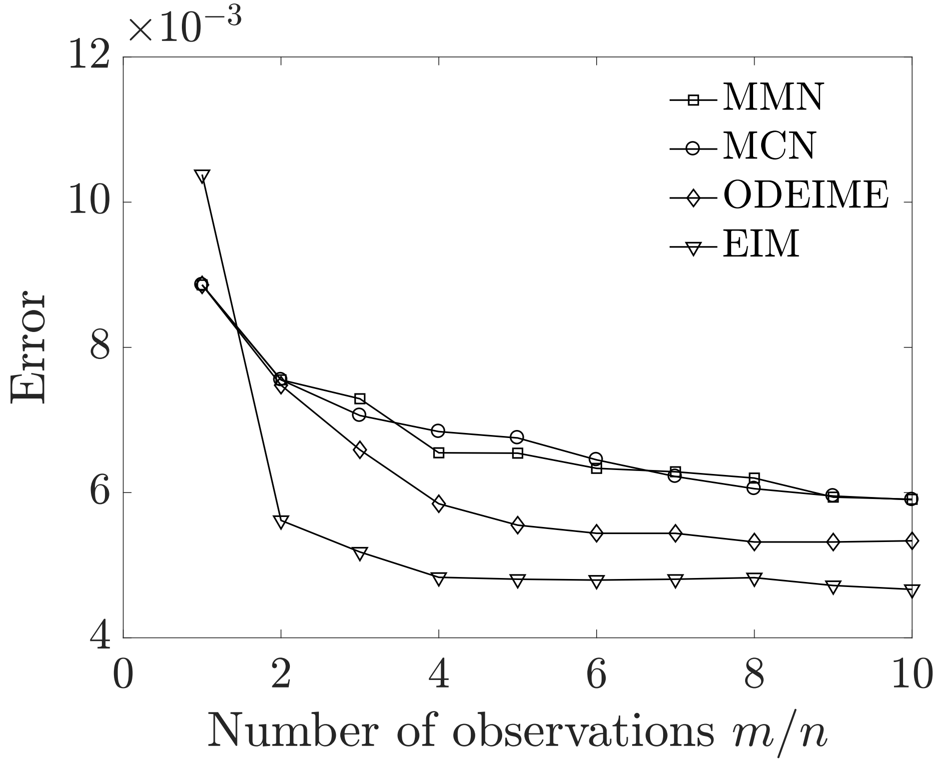

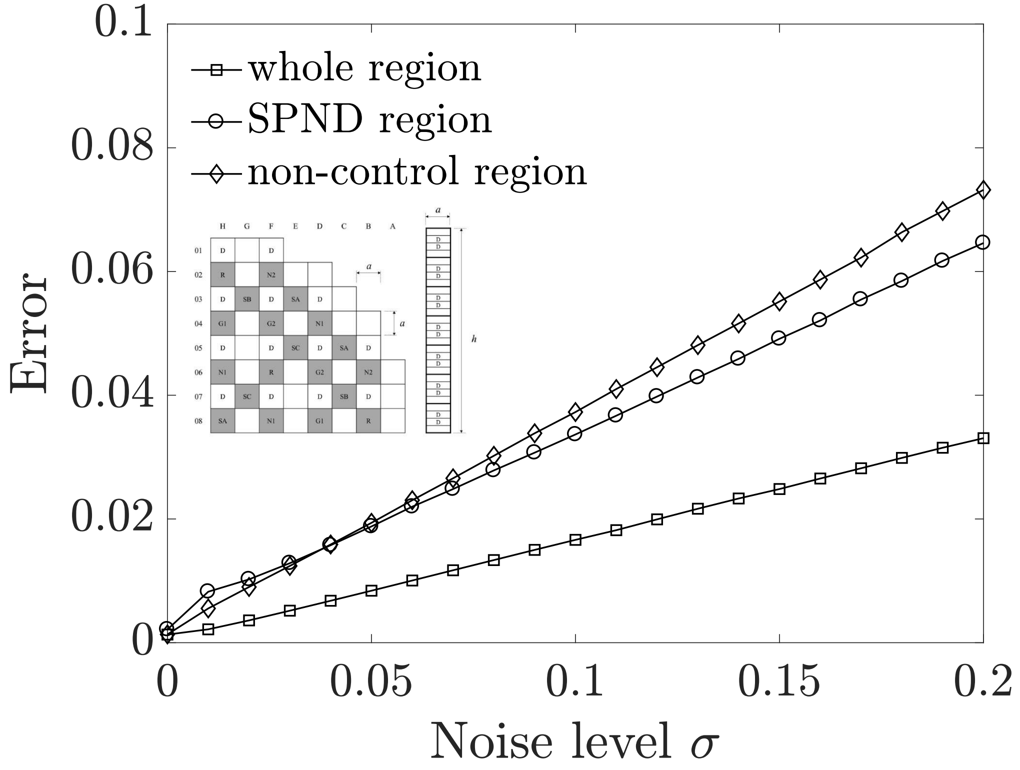

SPND = Self-Powered Neutron Detector
whole region: all candidate locations
SPND region: detector-accessible locations
non-control region: control-rod area excluded

Placement restrictions increase the reconstruction error under noise.

field error ↓ → safety-parameter uncertainty ↓

[Gong et al., NED, 2021]

PART II

Stabilized finite-information reconstruction

Finite-information reconstruction must be stabilized under measurement noise

Standard EIM/GEIM may lose convergence when sparse measurements are noisy

Algorithm 1: GEIM (Highlighting Error & Coefficient Links)

Input : Snapshot manifold $\mathcal{F} \subset \mathcal{V}$, Sensor dictionary Σ, Tolerance ε

Output : Reduced basis $\{q_1, \ldots, q_N\}$, Selected sensors $\{\ell_1, \ldots, \ell_N\}$

1 : Initialization ($n = 1$):

$$\varphi_1 = \arg\max_{\varphi \in \mathcal{F}} \|\varphi\|_{\mathcal{V}}$$

$$\ell_1 = \arg\max_{\ell \in \Sigma} |\ell(\varphi_1)|$$

$$q_1 = \varphi_1 \,/\, \ell_1(\varphi_1)$$

2 : **for** $n = 2, 3, \ldots, N_{\max}$ **do**

// Step 2.1: Greedy selection of the worst-approximated snapshot

$$\varepsilon_{n-1} := \max_{\varphi \in \mathcal{F}} \|\varphi - \mathcal{J}_{n-1}[\varphi]\|_{\mathcal{V}} \quad \Rightarrow \varphi_n$$

if $\varepsilon_{n-1} < \varepsilon$ **then break**

// Step 2.2: Greedy selection of the sensor maximizing the residual

$$\ell_n = \arg\max_{\ell \in \Sigma} |\ell(\varphi_n - \mathcal{J}_{n-1}[\varphi_n])|$$

// Step 2.3: Construct and normalize the new basis function

$$q_n = \frac{\varphi_n - \mathcal{J}_{n-1}[\varphi_n]}{\ell_n(\varphi_n - \mathcal{J}_{n-1}[\varphi_n])}$$

3 : **end for**

[Maday & Mula, Springer, 2013]

Link to : CS – GEIM Constraint
Bounded by: $|c_i| \leq \alpha(1 + \Lambda_{i-1})\varepsilon_{i-1}$

$$\mathcal{J}_{n-1}[\varphi] := \sum_{j=1}^{n-1} c_j q_j$$

$$\text{s.t. } \ell_i(\mathcal{J}_{n-1}[\varphi]) = \ell_i(\varphi)$$

Link to : Error Decay Curve
Drives the decreasing error ε

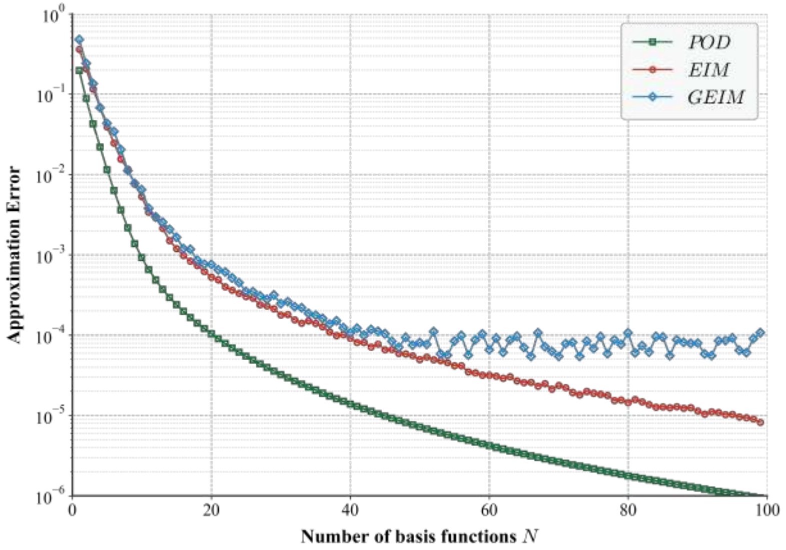

Constraint Set $\mathcal{K}_n$ in Subspace V_n

$$|c_i| \leq \alpha(1 + \Lambda_{i-1})\varepsilon_{i-1}$$

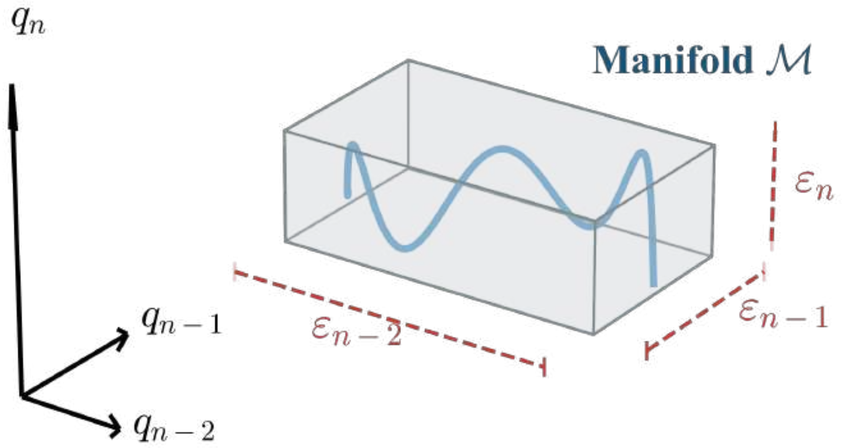

Finite-information reconstruction must be stabilized under measurement noise

Standard EIM/GEIM may lose convergence when sparse measurements are noisy

Constrained Stabilized GEIM (CS – GEIM) Formulation

Given: Noisy measurement vector $\mathbf{y}^\delta$, where $y_i^\delta = \ell_i(\varphi) + \eta_i$

Find: The stabilized reduced-order reconstruction $u_n^\delta = \sum_{j=1}^{n} c_j^\delta q_j$

where the coefficient vector $\mathbf{c}^\delta = (c_1^\delta, \dots, c_n^\delta)^T$ solves the inverse problem:

$$\mathbf{c}^\delta = \arg\min_{\mathbf{c}\in\mathcal{K}_n} \|\mathbf{L}_n\mathbf{c} - \mathbf{y}^\delta\|_{\ell^2}^2$$

with observation matrix $(\mathbf{L}_n)_{i,j} = \ell_i(q_j)$

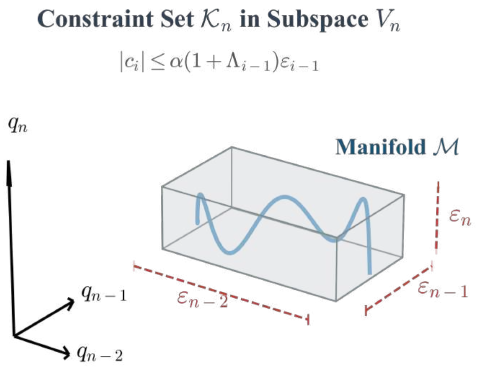

Subject to: *The manifold-informed constraint set $\mathcal{K}_n$:*

$$\boxed{\mathcal{K}_n = \{\mathbf{c} \in \mathbb{R}^n \mid |c_i| \le \alpha(1+\Lambda_{i-1})\varepsilon_{i-1},\ \forall i = 1, \dots, n\}}$$

[Argaud et al., ICOSAHOM, 2017; Gong, Sorbonne Univ., 2018]

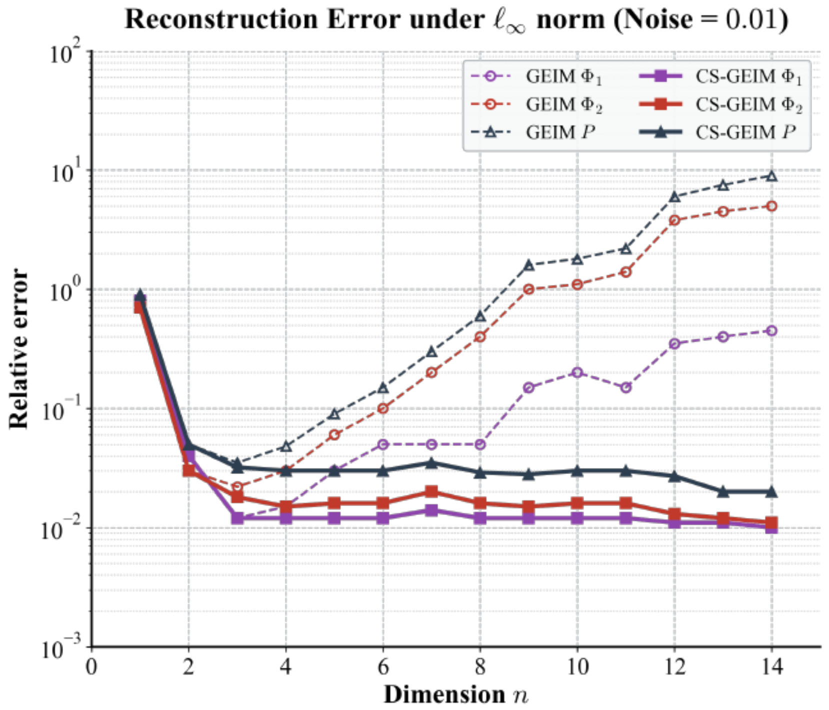

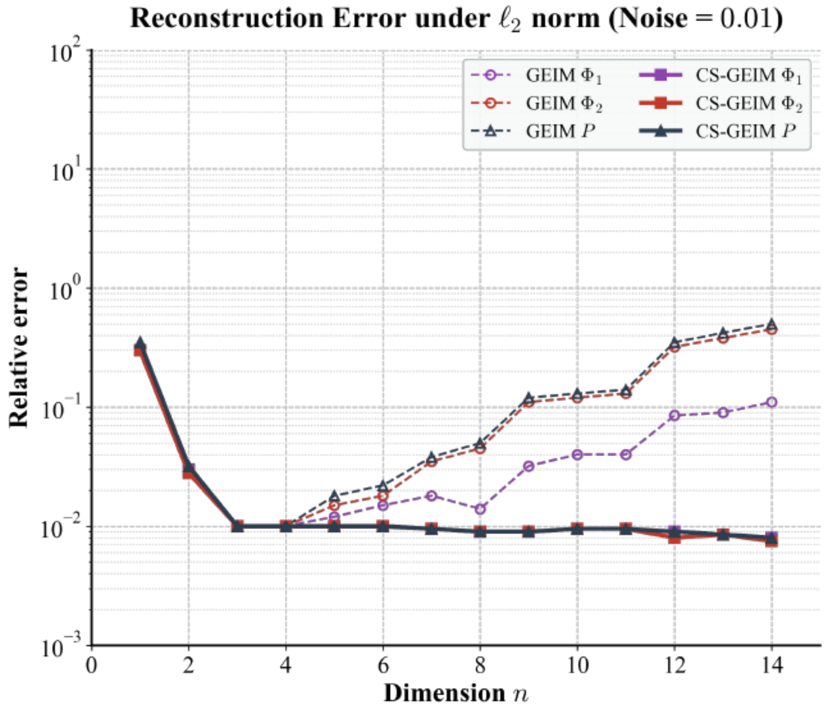

Regularized reduced bases improve stability in reactor-core field reconstruction

Weighted coefficient recovery controls noise amplification in online reconstruction

General Regularized RB Online Reconstruction

Finite Observations $\longrightarrow$ Weighted Coefficient Recovery $\longrightarrow$ Stable Field

To avoid noise amplification, solve the regularized inverse problem:

$$\mathbf{c}^{\delta} = \arg\min_{\mathbf{c}\in\mathbb{R}^n} \left\{ \|\mathbf{L}_n\mathbf{c} - \mathbf{y}^{\delta}\|_2^2 + \lambda \|\mathbf{W}\mathbf{c}\|_2^2 \right\}$$

where $\mathbf{L}_n$ is the observation matrix, and λ is the penalty parameter.

Basis Regularization Weights:

$\mathbf{W} = \mathrm{diag}(w_1, w_2, \ldots, w_n)$ where w_i penalizes instability.

- **For POD:** $w_i \propto \frac{1}{\sigma_i}$ (Inverse of SVD singular values)
- **For (G)EIM:** $w_i \propto \frac{1}{\max|c_i|}$ (Inverse of max EIM coefficients)

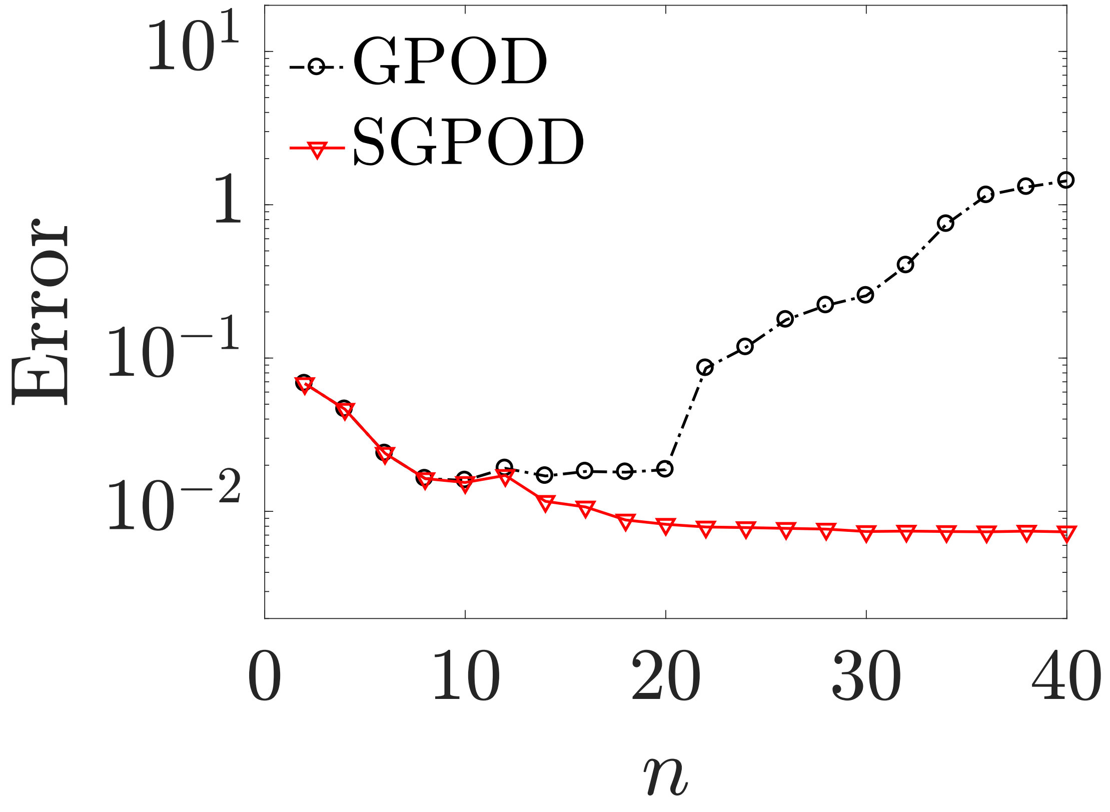

[Gong et al., NED, 2020; Gong et al., NED, 2021]

Remark: Regularization converts finite observations into stable reduced coefficients rather than noise-amplified interpolation.

Neural-Network-Augmented (G)EIM with Noise and Vibration Tolerance

Learning from data with models: $y^o \to u(\mu)$, with sparse noisy and movable sensors

EIM – based coefficient learning under perturbed observations

Noisy/movable sensors $\longrightarrow$ NN coefficient map $\longrightarrow$ Stable reduced reconstruction

Observation model: $\mathbf{y}^\delta = \mathbf{S}_{\Delta r}\,\mathbf{u} + \varepsilon$

Coefficient recovery: $\mathbf{c}^\delta = \mathcal{N}_\theta(\mathbf{y}^\delta)$

Reduced reconstruction: $\hat{\mathbf{u}} = \Phi\,\mathbf{c}^\delta$

The EIM basis reconstructs the field; the network maps perturbed measurements to coefficients.

Training with noise and vibration augmentation

$$\delta = \delta_{\text{noise}} + \delta_{\text{vibration}}$$
$$\mathcal{L}_{\text{train}} = \mathcal{L}_{\text{field}} + \lambda\,\mathcal{L}_{\text{Tik}}$$
$$\mathcal{N}_\theta : \mathbb{R}^m \to \mathbb{R}^n, \qquad \mathbf{y}^\delta \mapsto \mathbf{c}^\delta$$

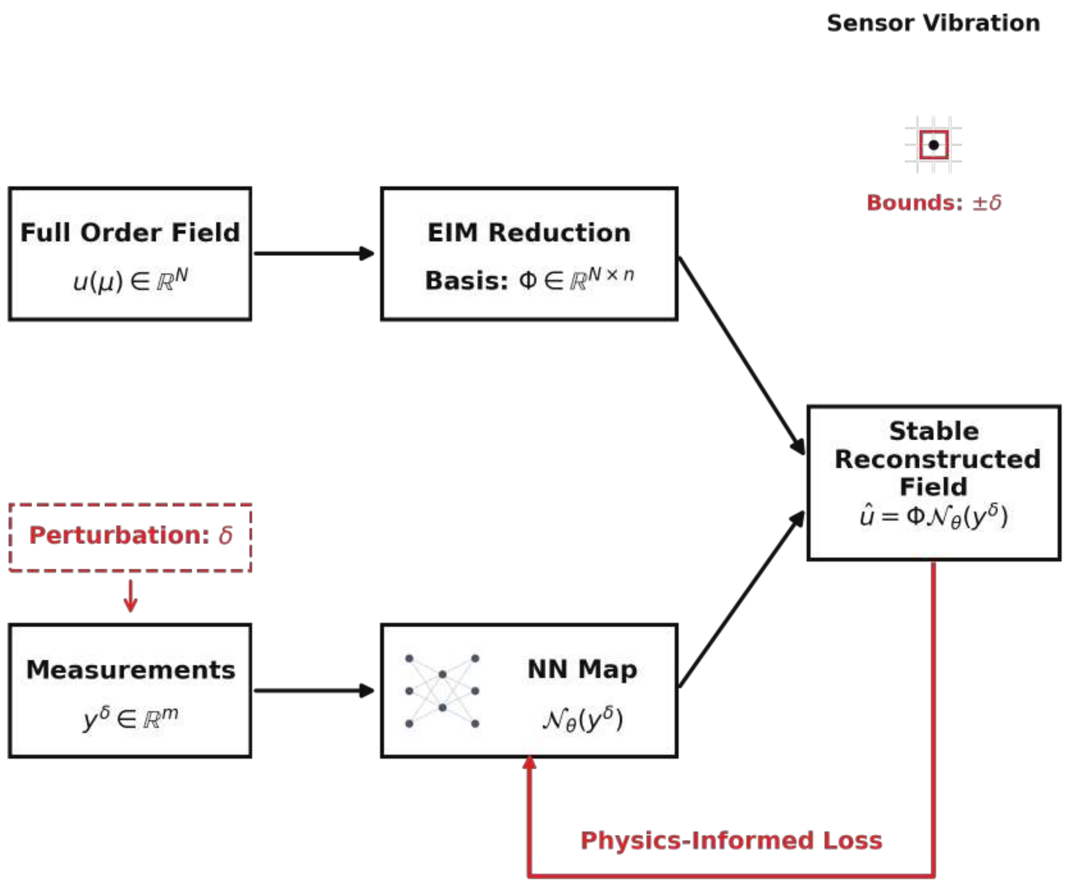

[Gong et al., NST, 2024; Xu et al., NSE, 2024;Li et al., CiCP, 2024,2026]

Coefficient-space learning improves noise and vibration tolerance

Benchmark-field evidence for EIM-NN / EIM-TNN under perturbed observations

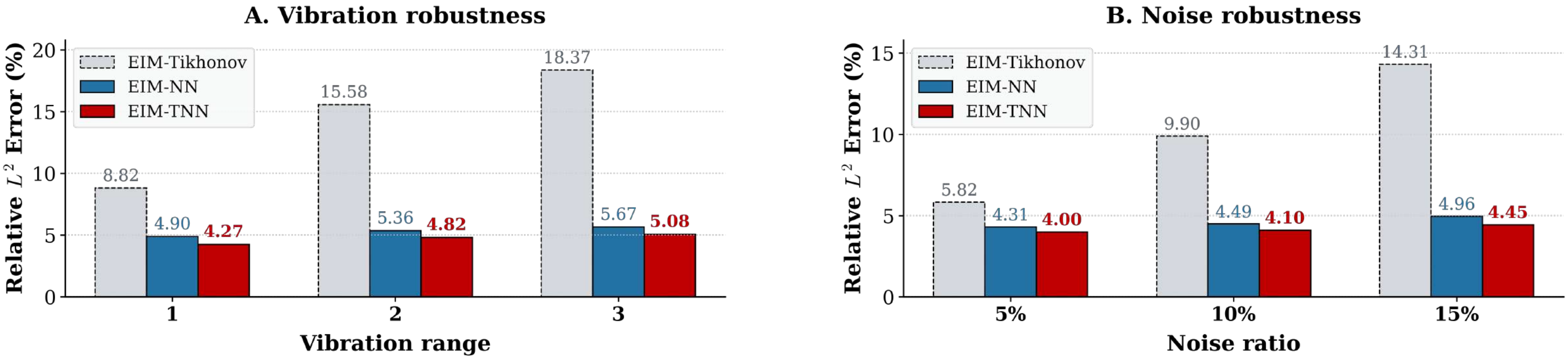

EIM-Tikhonov: linear EIM coefficient recovery with Tikhonov regularization.
EIM-NN: neural mapping from perturbed observations to EIM coefficients;
EIM-TNN: EIM-NN trained with Tikhonov-guided loss.

[Li, Gong & Xu, CiCP, 2026]

EIM-TNN keeps the relative L^2 error nearly unchanged under increasing observation noise and sensor vibration, while the linear EIM-Tikhonov reconstruction degrades rapidly. The improvement comes from learning the EIM coefficients under perturbed observations, with the EIM basis still used for field reconstruction.

PART III

Model mismatch and parameter/state estimation

PBDW provides a rigorous geometric foundation for reduced model–data fusion

An open question in reactor physics is how to extend this framework under physical model error

Neutron Transport Equation

(High-Fidelity Physical Truth $\Rightarrow u^{\text{true}}$)

$$\hat{\Omega} \cdot \nabla \psi(\vec{r}, \hat{\Omega}, E) + \Sigma_t(\vec{r}, E)\psi(\vec{r}, \hat{\Omega}, E) = Q_{scatter} + Q_{fission}$$

Angular Flux ψ: Space(3D) + Angle(2D) + Energy(1D) = 6D

Approximations:

Angle: Fick's Law

Energy:Condensation

Induces Model Discrepancy δ

Two-Group Diffusion Equation

(Reduced Background Model $\Rightarrow V_N$)

$$-\nabla \cdot (D_1 \nabla \phi_1) + \Sigma_{R1}\phi_1 = \frac{1}{k_{eff}}(\nu\Sigma_{f1}\phi_1 + \nu\Sigma_{f2}\phi_2)$$

$$-\nabla \cdot (D_2 \nabla \phi_2) + \Sigma_{a2}\phi_2 = \Sigma_{1\to 2}\phi_1$$

Scalar Flux ϕ: Space(3D) = 3D

Two sources of inaccuracy: model discrepancy and parameter uncertainty

Model bias changes the solution manifold, while parameter uncertainty changes the distribution of reactor states

Model discrepancy

Sources:
- transport truth vs diffusion background
- missing physics / approximation / closure error

$$u^{\text{true}} = u^{\text{model}} + \delta_{\text{model}}$$

or: $\mathcal{F}_{\text{true}}(u,\mu) = 0, \quad \mathcal{F}_{\text{ROM}}(u,\mu) = 0$

Method path:

PBDW-inspired fusion + learned discrepancy correction

background reduced space + observations $\longrightarrow$ *corrected state + learned* δ

Key point:

Not a parameter estimation error, but a systematic bias due to model simplification.

Parameter uncertainty

Sources:
- cross sections / material constants
- operating parameters / boundary conditions

$$\mu \sim \pi(\mu)$$

$\pi(\mu) \rightarrow \pi(\mu \mid y)$ (after observations)

Method path:

Ensemble Bayesian parameter distribution inference

prior distribution + sensor observations $\longrightarrow$ *posterior frequency distribution* $\longrightarrow$ *updated parameter uncertainty*

Key point:

Not a point estimate $\hat{\mu}$, but a full distribution $\rightarrow$ suitable for BEPU uncertainty propagation.

$\delta_{\text{model}} \downarrow$ $\qquad$ $\pi(\mu \mid y)$ updated $\downarrow$

$$\Rightarrow P(M(u,\mu,t) > 0 \mid y) \ \textbf{more credible}$$

Both routes reduce uncertainty in the final safety-margin probability,but they act on different parts of the inference chain.

PBDW provides a rigorous geometric foundation for reduced model–data fusion

An open question in reactor physics is how to extend this framework under physical model error

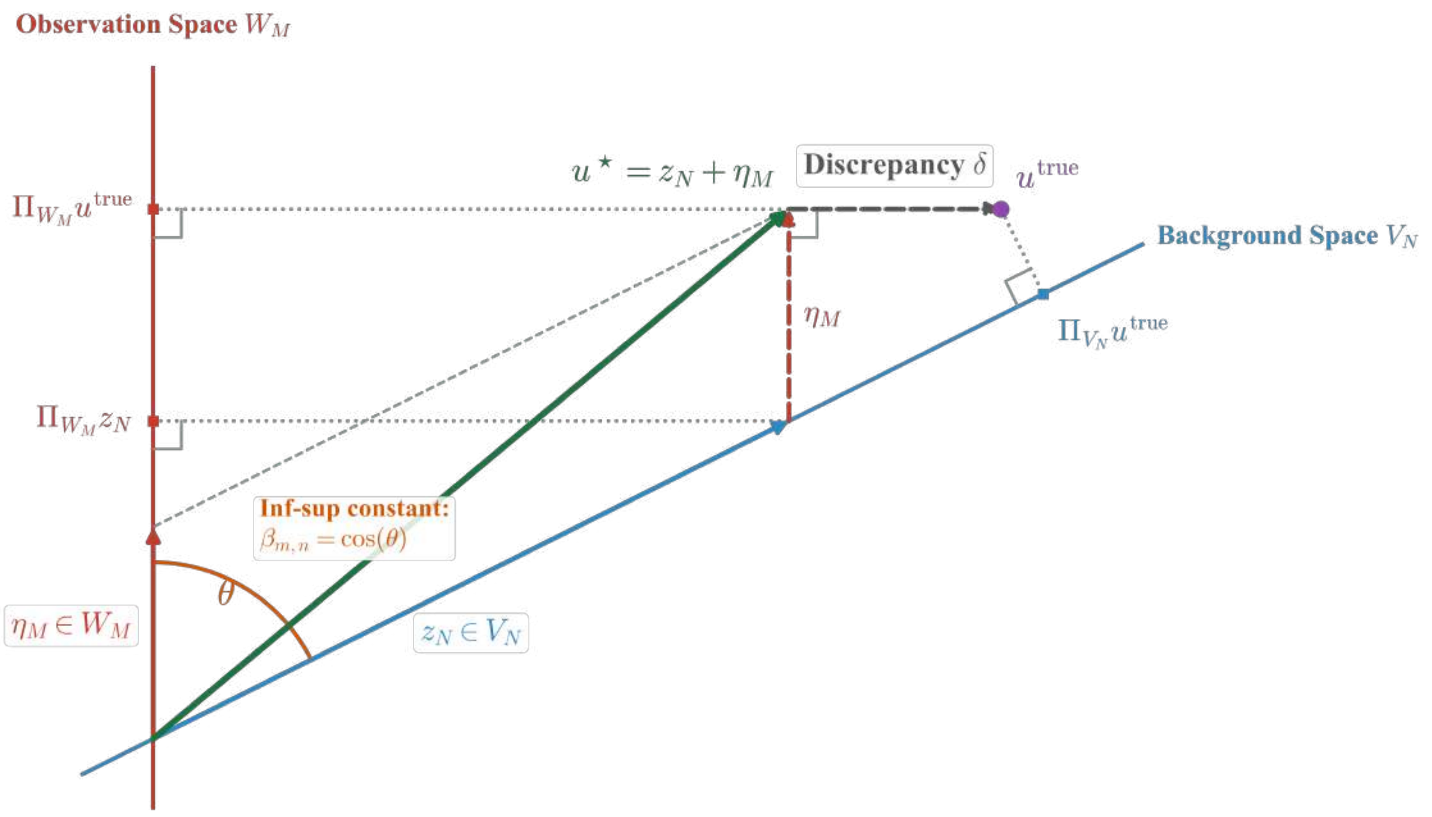

See also: Taumhas et al., ESAIM Proc. Surv., 2023

Parametrized-Background Data-Weak (PBDW) Formulation

Given : Reduced background space $V_N \subset \mathcal{U}$ and observation space $W_M \subset \mathcal{U}$

Find : Background component $z_N^\star \in V_N$ and update $\eta_M^\star \in W_M$ satisfying:

$$(\eta_M^\star, w)_{\mathcal{U}} + (z_N^\star, w)_{\mathcal{U}} = \langle \mathbf{y}, w \rangle \qquad \forall w \in W_M$$ ← Data Matching in W_M

$$(\eta_M^\star, v)_{\mathcal{U}} = 0 \qquad \forall v \in V_N$$ ← Orthogonality to V_N

Output : $\boxed{u^\star = z_N^\star + \eta_M^\star}$

Stability : Well-posedness is governed by the inf-sup constant $\beta_{M,N}$:

$$\beta_{M,N} := \inf_{v \in V_N} \sup_{w \in W_M} \frac{(v, w)_{\mathcal{U}}}{\|v\|_{\mathcal{U}} \|w\|_{\mathcal{U}}} > 0$$

[Maday et al., IJNME, 2015]

Future work

Ensemble Bayesian inference for parameter distributions

Updating prior distributions reduces parameter uncertainty for data assimilation and margin assessment

Ensemble Bayesian inference

for parameter distributions

prior distribution

$\pi(\mu)$

sensor observations

y_i

reactor model

$f(r, \mu)$

$\downarrow$

MCMC / Ensemble Bayesian sampling

$\downarrow$

posterior frequency distribution

$\pi(\mu \mid y)$

$$p(\mu_j \mid y_{1,j}, \ldots, y_{m,j}) \propto \pi(\mu_j) \prod_{i=1}^{m} p(y_{i,j} \mid \mu_j)$$

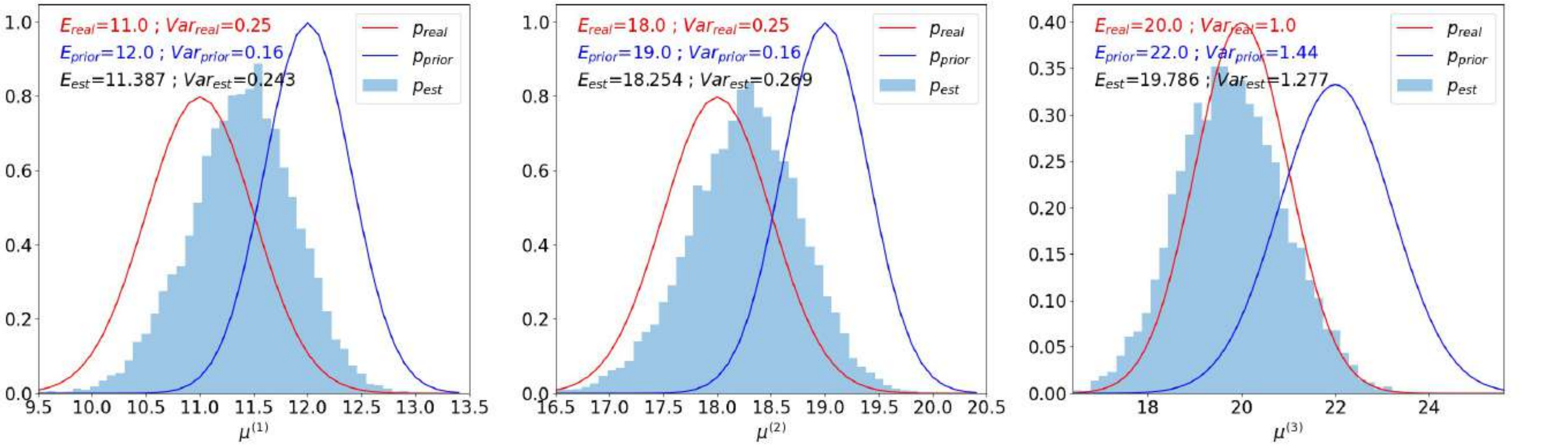

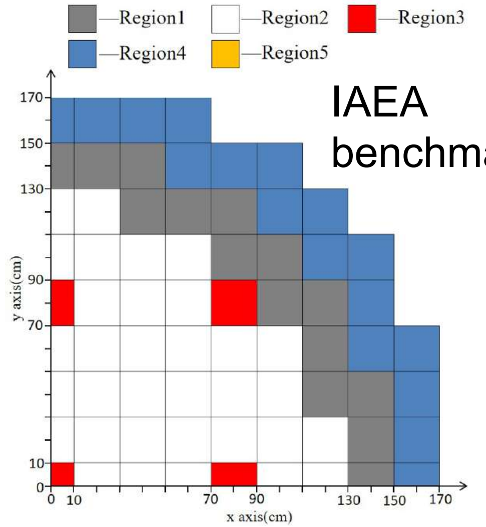

IAEA benchmark

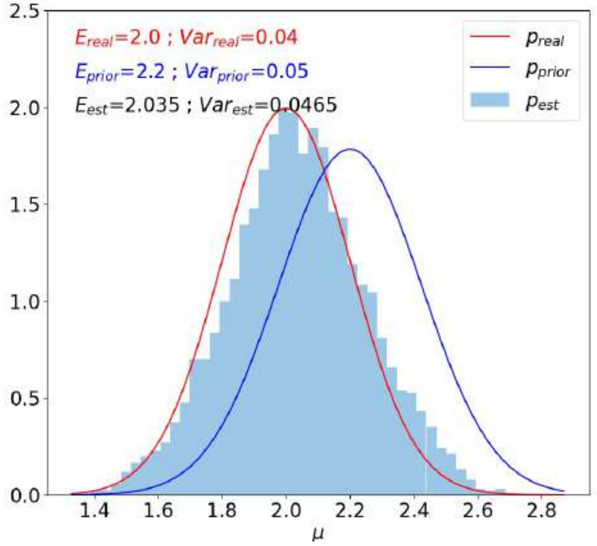

From prior to posterior, uncertain parameters are constrained by observations before being used in ROM inference.

Remark: Parameter distributions, rather than single best estimates, allow the digital twin to carry uncertainty into BEPU-style margin assessment.

[Zeng et al., NST, 2023]

PART IV

Nonlinear reduced coordinates

Example of nonlinear multi-physics problem

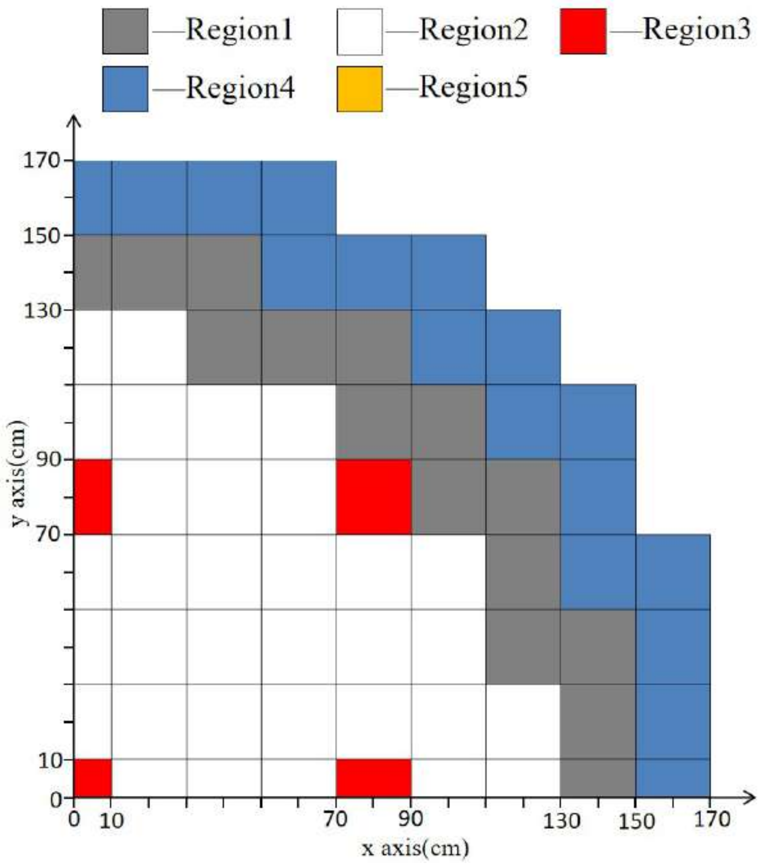

Power density as heat source:

$$P(\mathbf{x}) \quad = \quad \tilde{c}\sum_{g=1}^{2} \kappa\Sigma_{f,g}(\mathbf{x})\phi_g(\mathbf{x})$$

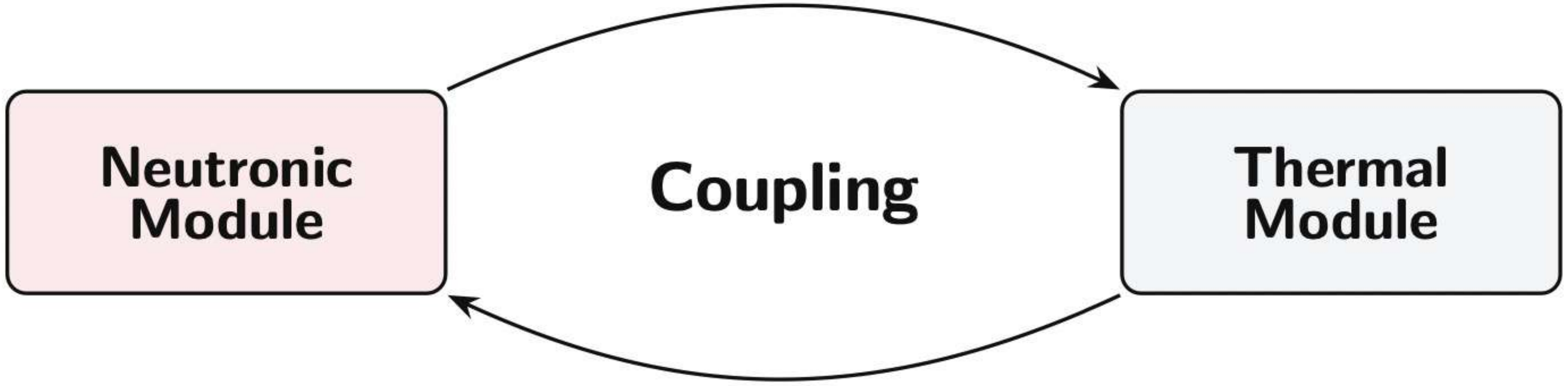

Temperature feedback on diffusion coefficients and macroscopic absorption cross sections:

$$D_g \quad = \quad f_D\left(T;\ T^{\mathrm{ref}}, D_g^{\mathrm{ref}}, \gamma_D\right), \quad g \quad = \quad 1,2$$
$$\Sigma_{a,g} \quad = \quad f_a\left(T;\ T^{\mathrm{ref}}, \Sigma_{a,g}^{\mathrm{ref}}, \gamma_a\right), \quad g \quad = \quad 1,2$$

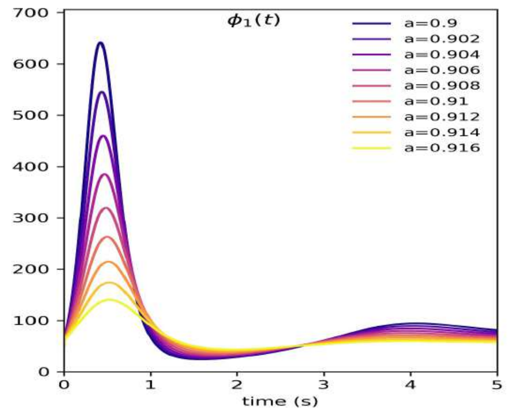

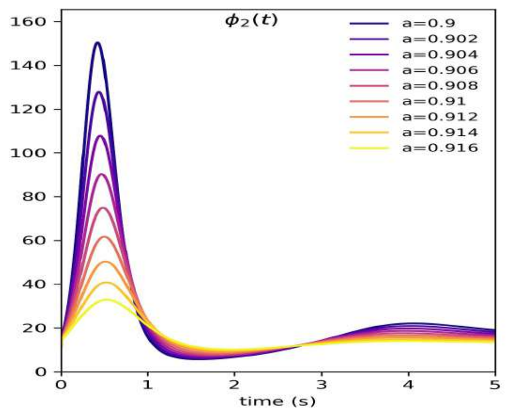

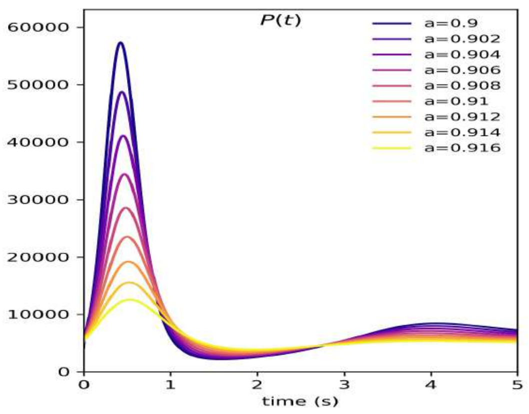

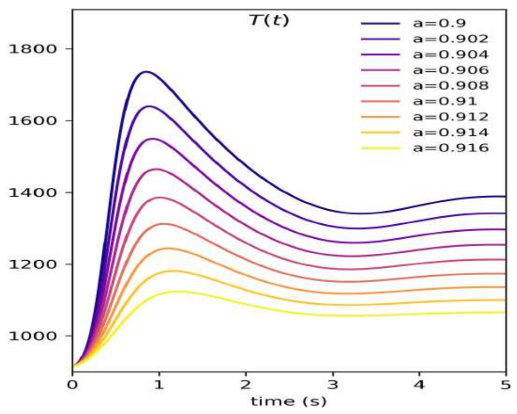

Example of nonlinear multi-physics problem

- **Two-Group Neutron Kinetics (with Precursor Feedback):**

$$\frac{1}{v_1}\frac{\partial \phi_1}{\partial t} = \nabla \cdot D_1(T)\nabla\phi_1 - \Sigma_{r1}(T)\phi_1 + \frac{1-\beta}{k_{\text{eff}}}\sum_{g=1}^{2}\nu\Sigma_{fg}\phi_g + \lambda C$$

$$\frac{1}{v_2}\frac{\partial \phi_2}{\partial t} = \nabla \cdot D_2(T)\nabla\phi_2 - \Sigma_{a2}(T)\phi_2 + \Sigma_{s,1\to 2}\phi_1$$

- **Power Generation & Thermal-Hydraulics Heat Equation:**

$$P(\vec{r},t) = \kappa\sum_{g=1}^{2}\Sigma_{fg}\phi_g$$

$$\rho c_p\frac{\partial T}{\partial t} = \nabla \cdot K\nabla T + P(\vec{r},t) - q_{\text{cool}}(T)$$

Cross-Field Parameter Feedback (Doppler & Moderator Effects):

$$T(\vec{r},t) \;\Rightarrow\; \Sigma_{a,g}(T) = \Sigma^0_{a,g} + \gamma_a\sqrt{T}, \quad D_g(T) = D^0_g + \gamma_D T$$

Reactor-scale: HPR1000 xenon oscillation

Long-term delayed coupling in 3D core dynamics

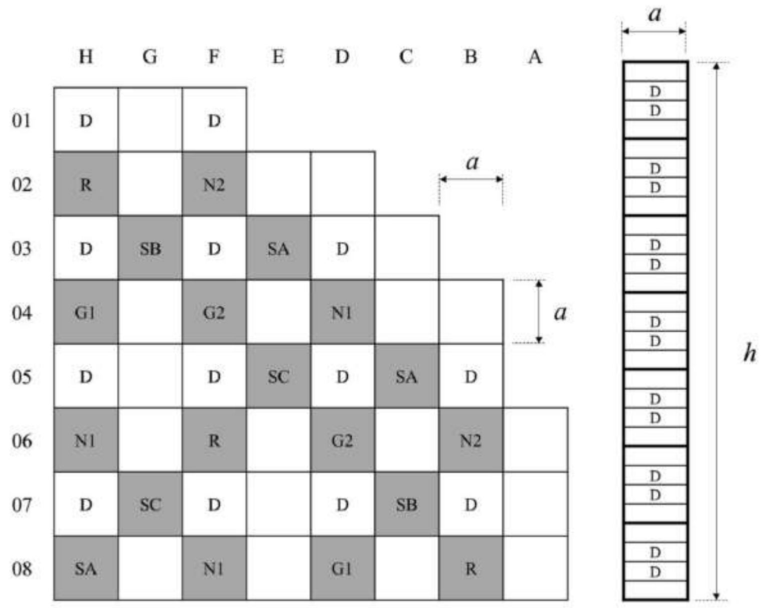

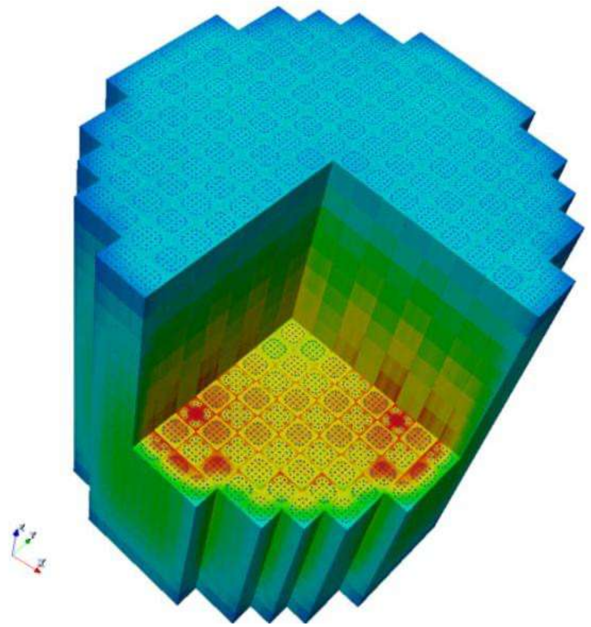

HPR1000 xenon oscillation

Governing Multiphysics System & Sparse Observation

Neutronics: $$\frac{1}{v}\frac{\partial\phi}{\partial t} = \nabla\cdot(D\nabla\phi) + \left[(1-\beta)\nu\Sigma_f - \Sigma_a(T) - \sigma_a^X X_e(\phi)\right]\phi + \lambda C$$

Thermal-Hydraulics: $$\rho C_p\frac{\partial T}{\partial t} + \rho C_p\vec{u}\cdot\nabla T = \nabla\cdot(k\nabla T) + \kappa\Sigma_f\phi$$

Isotope Poisoning: $$\frac{\partial I}{\partial t} = \gamma_I\Sigma_f\phi - \lambda_I I, \quad \frac{\partial X_e}{\partial t} = \gamma_X\Sigma_f\phi + \lambda_I I - (\lambda_X + \sigma_a^X\phi)X_e$$

Sparse Observation: $$\mathcal{Y}_{\mathrm{obs}}(t) = \mathbf{C}_{\mathrm{sparse}}\cdot\phi(\vec{r}_{\mathrm{sensor}}, t) + \epsilon$$

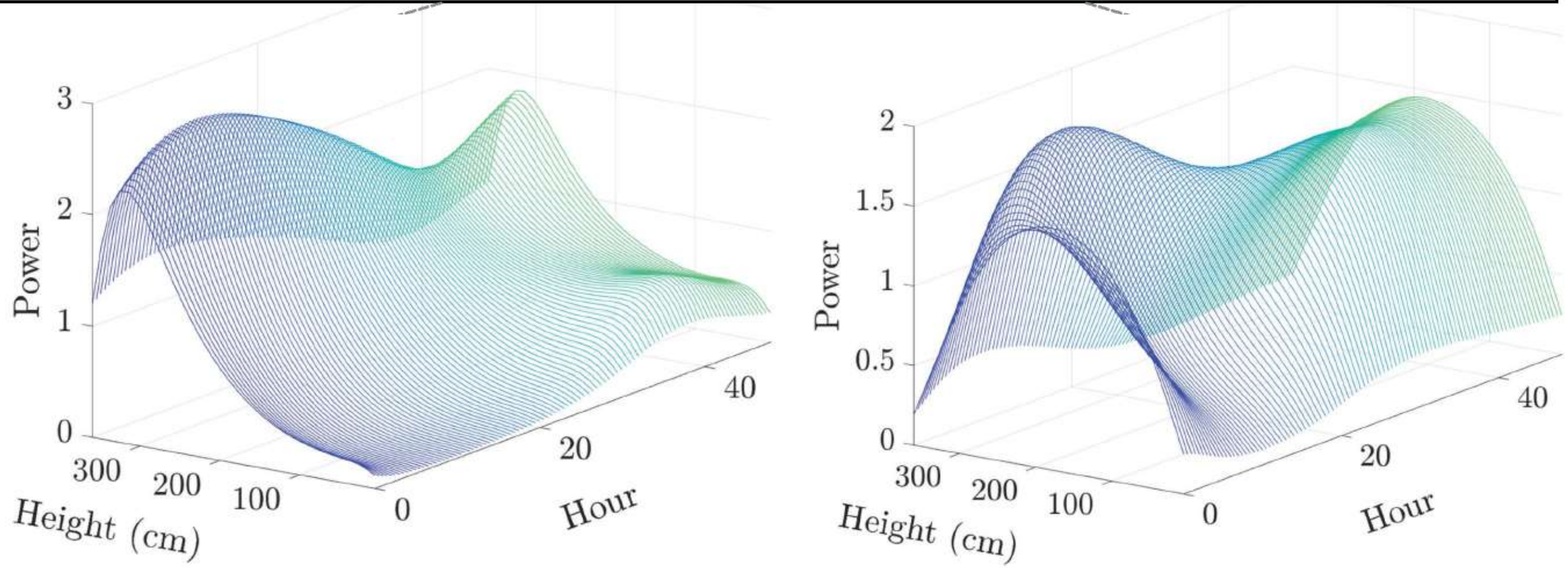

[Bao et al., JCP, 2025]

Nonlinear transient manifolds challenge linear reduced spaces

Coupled reactor dynamics bend the solution geometry, motivating latent coordinates beyond POD

IAEA 2D N-TH Benchmark Equation System

1. Spatiotemporal Full-Order State Vector

The high-fidelity coupled system is defined by grouping the neutronics and thermal-hydraulics fields into a monolithic snapshot matrix:

$$\mathcal{U}(\vec{r},t) = [\,\phi_1(\vec{r},t),\ \phi_2(\vec{r},t),\ P(\vec{r},t),\ T(\vec{r},t)\,]^\top \in \mathbf{R}^{4\times N_{\text{space}}}$$

2. Nonlinearly Coupled Governing Operators

- **Two-Group Neutron Kinetics (with Precursor Feedback):**

$$\frac{1}{v_1}\frac{\partial \phi_1}{\partial t} = \nabla\cdot D_1(T)\nabla\phi_1 - \Sigma_{r1}(T)\phi_1 + \frac{1-\beta}{k_{\text{eff}}}\sum_{g=1}^{2}\nu\Sigma_{fg}\phi_g + \lambda C$$

$$\frac{1}{v_2}\frac{\partial \phi_2}{\partial t} = \nabla\cdot D_2(T)\nabla\phi_2 - \Sigma_{a2}(T)\phi_2 + \Sigma_{s,1\to 2}\phi_1$$

- **Power Generation & Thermal-Hydraulics Heat Equation:**

$$P(\vec{r},t) = \kappa\sum_{g=1}^{2}\Sigma_{fg}\phi_g$$

$$\rho c_p\frac{\partial T}{\partial t} = \nabla\cdot K\nabla T + P(\vec{r},t) - q_{\text{cool}}(T)$$

Cross-Field Parameter Feedback (Doppler & Moderator Effects):

$$T(\vec{r},t)\ \Rightarrow\ \Sigma_{a,g}(T) = \Sigma^0_{a,g} + \gamma_a\sqrt{T},\quad D_g(T) = D^0_g + \gamma_D T$$

3. Nonlinear Geometry & Subspace Decay Bottleneck

Transient snapshots form a state manifold $\mathcal{S}_{\text{train}} = \{\mathcal{U}_1,\ \ldots,\mathcal{U}_{N_s}\}$.
Strong multi-physics feedback warps the solution into a curved manifold $\mathcal{M}$.
Linear methods (POD) suffer spectral dilution; nonlinear reduction is required.

[Bao et al., JCP, 2025]

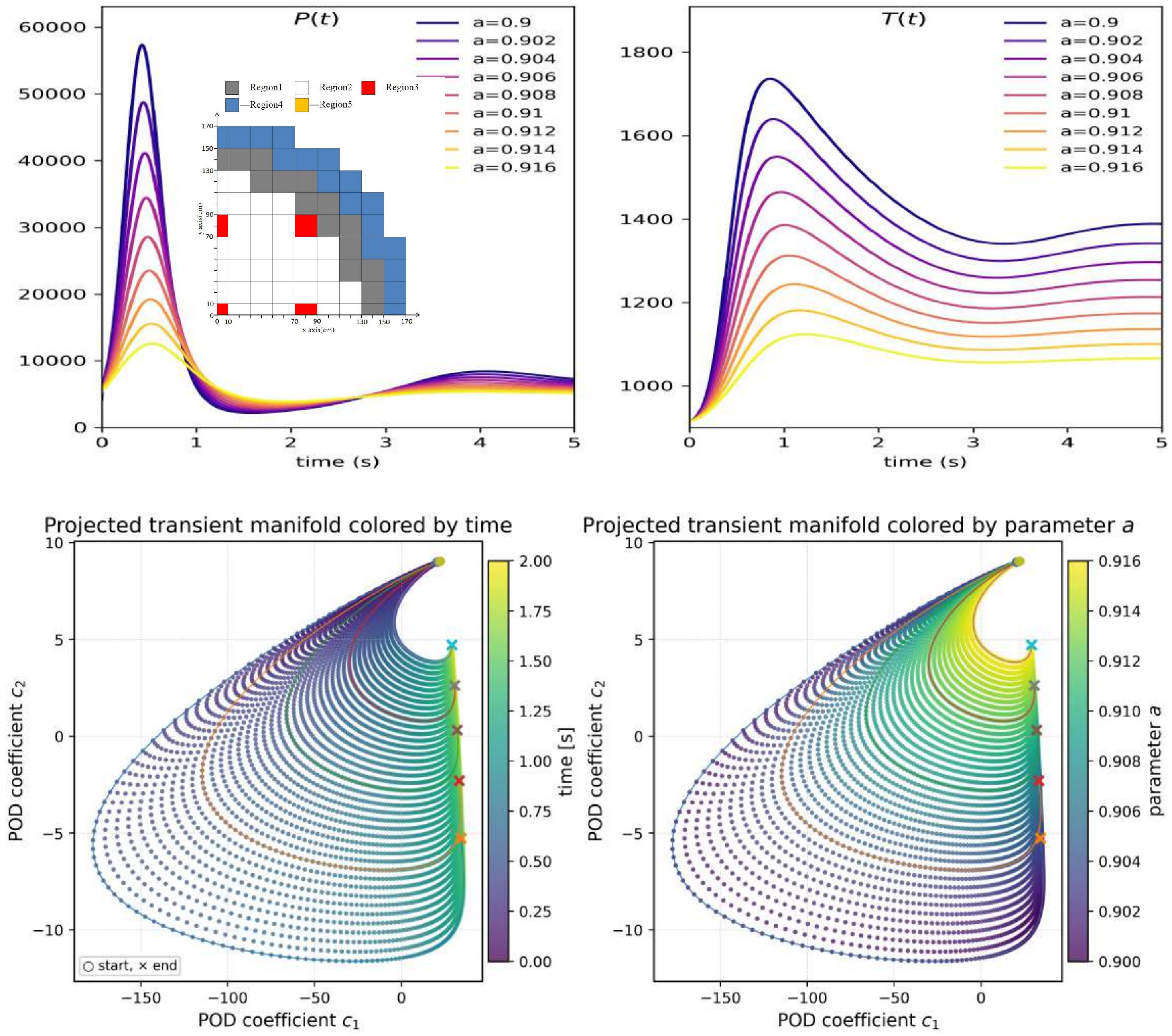

Two nonlinear coordinates capture the transient manifold more efficiently than POD

A 2D latent state reaches the accuracy of several linear POD modes in a coupled benchmark

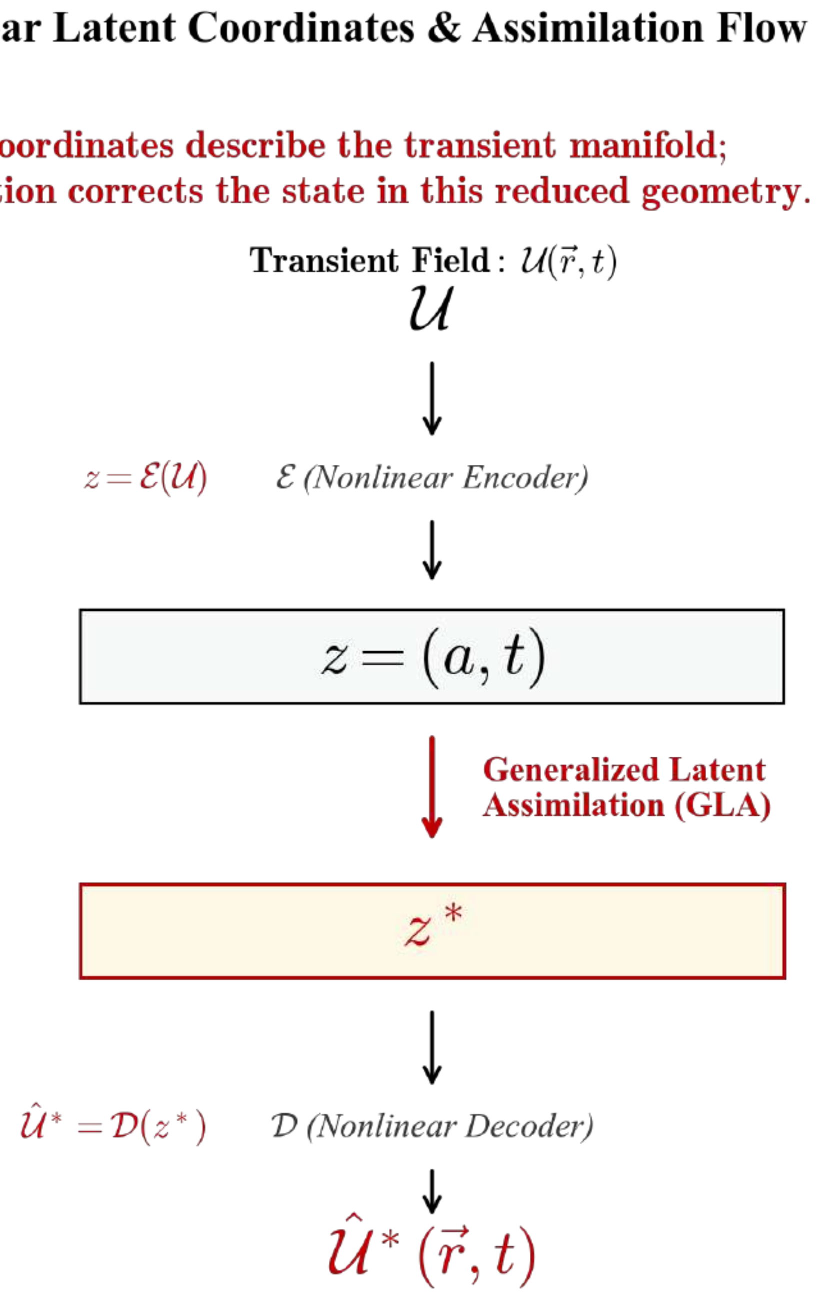

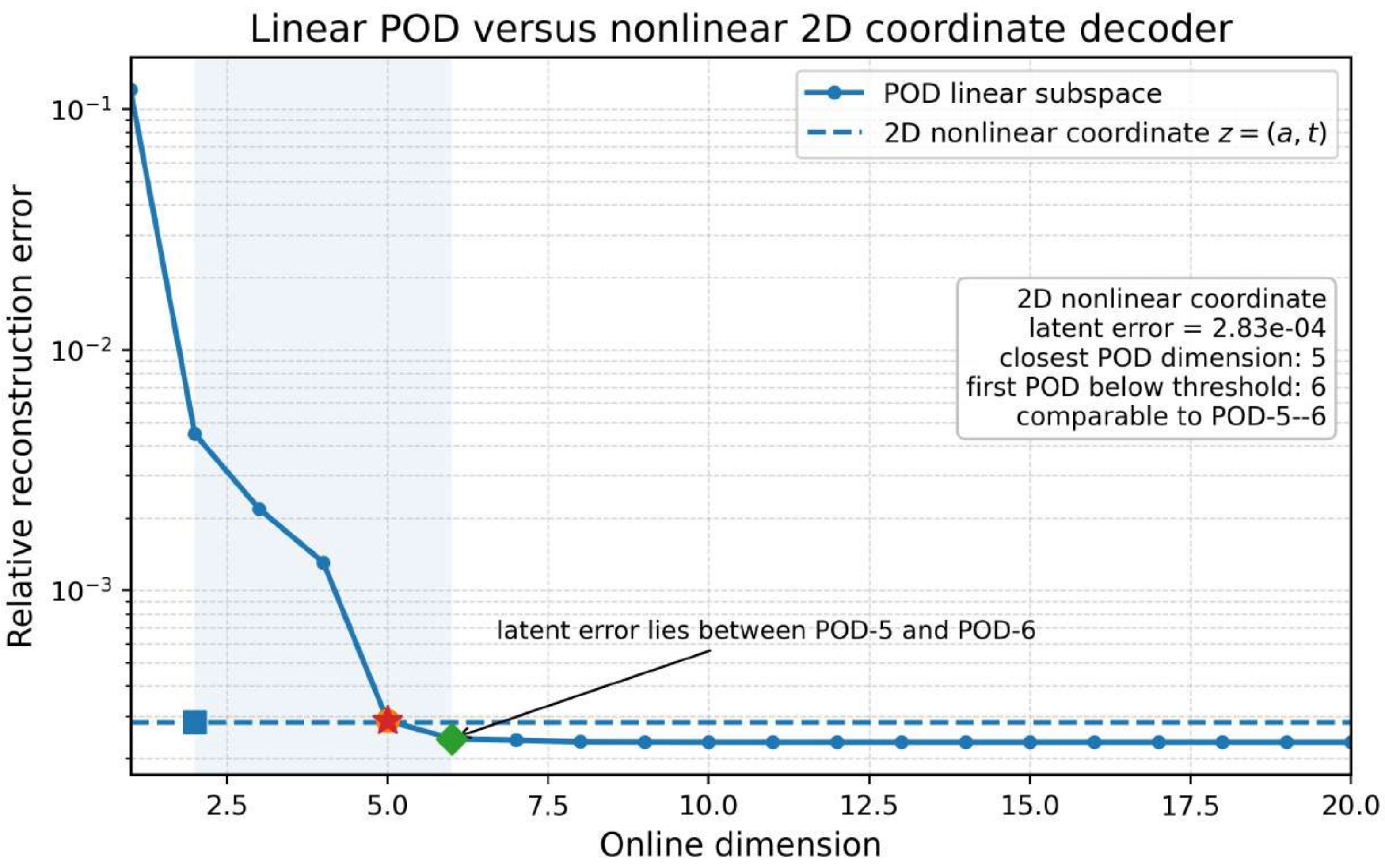

- Same online dimension: 2D nonlinear coordinate << POD-2 error
- Comparable global accuracy: 2D coordinate ≈ POD-5–6
- Meaning: nonlinear state geometry reduces online dimension

Latent coordinates turn sparse observations into field corrections

SVD-AE builds the nonlinear reduced state; GLA updates it online before decoding back to the field

1. Two-Stage Nonlinear Compression (Forward Kinematics)

High−Fidelity Field : $\mathcal{U}(\vec{r}, t) \in \mathbf{R}^{N_{\text{space}}}$

$\downarrow$ SVD/POD Projection

POD Coefficients : $\alpha = \mathbf{V}_n^{\top} \mathcal{U} \in \mathbf{R}^{500}$

$\downarrow$ $\mathcal{E}$: Nonlinear Encoder

Learned Latent State : $z = \mathcal{E}(\alpha) \in \mathbf{R}^{30}$

Two-Stage Reduction: 500 Coeffs → 30 Latent

$\downarrow$ $\mathcal{D}$: Nonlinear Decoder

Recovered Coefficients : $\hat{\alpha} = \mathcal{D}(z) \in \mathbf{R}^{500}$

$\downarrow$ $\mathbf{V}_n$: Basis Expansion

Reconstructed Field : $\hat{\mathcal{U}}(\vec{r}, t) = \mathbf{V}_n \hat{\alpha}$

2. Generalized Latent Assimilation (Inverse Flow)

Background Parameters/States : μ_b (or z_b)

$\downarrow$

Background Prediction : $\mathcal{U}_b = \mathcal{D}(z_b)$

$\downarrow$

Sparse Observations (y) from Core Sensors

GLA Online Correction

$$\min_z \|y - \mathcal{H}(\mathbf{V}_n \mathcal{D}(z))\|^2_{\mathbf{R}^{-1}} + \|z - z_b\|^2_{\mathbf{B}^{-1}}$$

$\downarrow$

Assimilated Latent/Parameters : z^* (or μ_a)

$\downarrow$

Assimilated Field : $\mathcal{U}_a(\vec{r}, t) = \mathbf{V}_n \mathcal{D}(z^*)$

$$\textbf{Manifold Reduction:} \quad z = \mathcal{E}(\alpha), \quad \hat{\alpha} = \mathcal{D}(z), \quad \hat{\mathcal{U}} = \mathbf{V}_n \hat{\alpha}$$

$$\textbf{Assimilation Flow:} \quad z \ (\text{or } \mu) \xrightarrow{\textbf{GLA} + \mathcal{H}(\mathbf{y})} z^* \ (\text{or } \mu_a) \xrightarrow{\textbf{Decoder Expansion}} \hat{\mathcal{U}}_a$$

[Gong et al., ANE, 2022]

Latent assimilation reduces full-space error at online cost

HPR1000-type tests show robust correction under observation noise with sub-second update time

Results on HPR1000 type

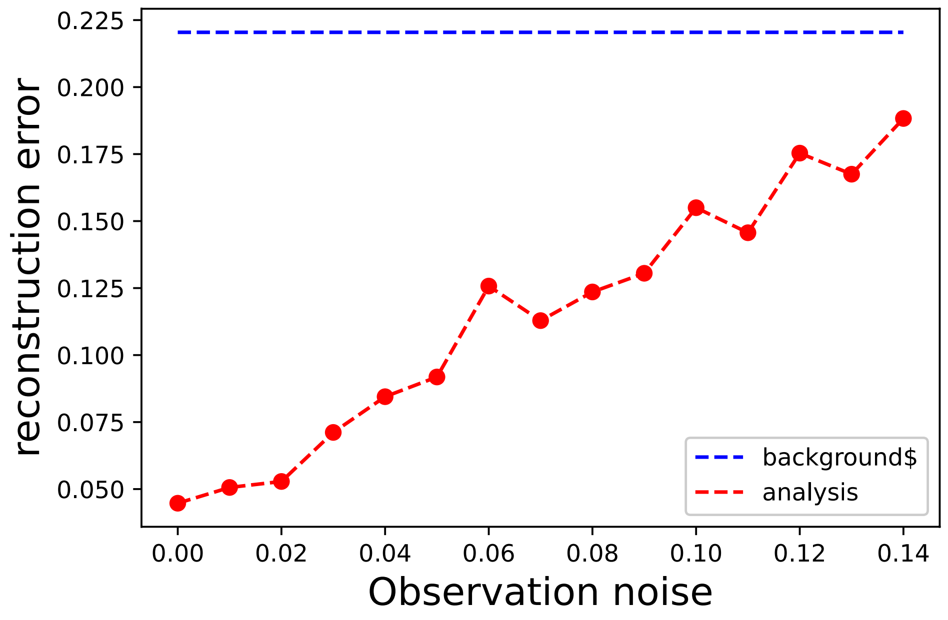

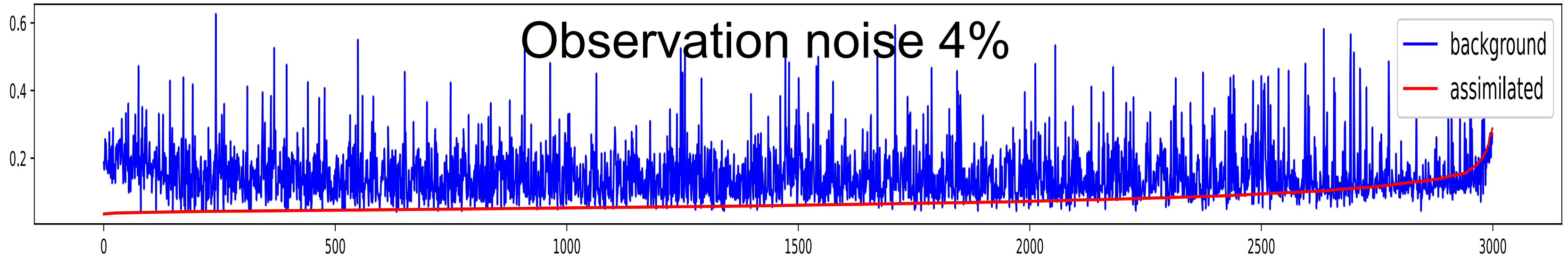

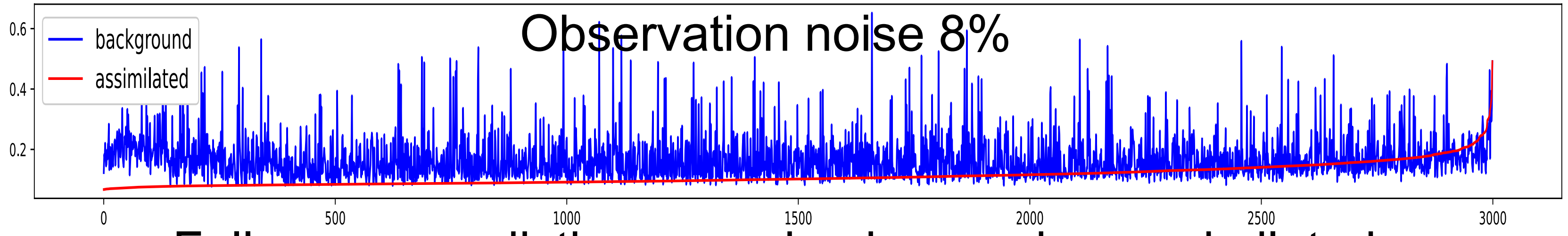

Full-space prediction error: background vs assimilated

Nonlinear Manifold Reduction

SVD-AE learns optimal nonlinear coordinates:

- Compresses 500 POD coefficients $\rightarrow$ 30 latent variables
- 20 latent variables are sufficient to reach best accuracy
- Standard linear POD needs >30 bases for comparable performance

Variational Latent Assimilation

GLA utilizes sparse observations to correct states:

- Background parameter / field error drops significantly
- Assimilated state ensures full-space physical field correction

$$y_b + \text{observations} \longrightarrow \mu_a \longrightarrow \mathcal{U}_a$$

Ultra-Real-Time Online Usability

Computational efficiency remains well below operational scale:

- **Forward Prediction (SVD – AE):** ~ 0.08 s
- **Inverse Update (GLA):** ~ 0.9 s
- **Traditional CORCA – 3D Ref:** ~ 40 s

[Gong et al., ANE, 2022]

PART V

Multi-field inference and trajectory forecasting

Cross-field inference under partial observations

A latent multi-physics map connects measured signals to safety-relevant fields

Governing Multiphysics System & Sparse Observation

$$\textbf{Neutronics:}\quad \frac{1}{v}\frac{\partial \phi}{\partial t} = \nabla\cdot(D\nabla\phi) + \left[(1-\beta)\nu\Sigma_f - \Sigma_a(T) - \sigma_a^X X_e(\phi)\right]\phi + \lambda C$$

$$\textbf{Thermal-Hydraulics:}\quad \rho C_p\frac{\partial T}{\partial t} + \rho C_p\vec{u}\cdot\nabla T = \nabla\cdot(k\nabla T) + \kappa\Sigma_f\phi$$

$$\textbf{Isotope Poisoning:}\quad \frac{\partial I}{\partial t} = \gamma_I\Sigma_f\phi - \lambda_I I,\quad \frac{\partial X_e}{\partial t} = \gamma_X\Sigma_f\phi + \lambda_I I - (\lambda_X + \sigma_a^X\phi)X_e$$

$$\textbf{Sparse Observation:}\quad \mathcal{Y}_{\text{obs}}(t) = \mathbf{C}_{\text{sparse}}\cdot\phi(\vec{r}_{\text{sensor}}, t) + \epsilon$$

Observed Field

$\mathcal{Y}_{\text{obs}}(t) \in \mathbb{R}^m$

- Ex-core / In-core Flux
- Loop Temperatures

→

Latent Manifold Space

$\mathcal{O}_{\text{latent}} : y \to \hat{u}_{\text{multi}} \to \hat{\mathcal{M}}$

- Non-linear Spatiotemporal SVD-AE
- Cross-Field Coupling Propagation

→

Safety Fields

$\hat{\mathcal{U}}_{\text{safe}}(t) \in \mathcal{V}_{\text{full}}$

- Peaking Factor ($F_Q \to T_{\text{fuel}}$)
- Safety Margin ($\hat{\mathcal{M}}, X_e$)

$$\textbf{Cross-Field Mapping:}\quad \mathcal{Y}_{\text{obs}}(t) \xrightarrow{\mathcal{E}_{\text{obs}}} z(t) \xrightarrow{\mathcal{D}_{\text{full}}} \hat{\mathcal{U}}_{\text{multi}}(\vec{r}, t) \implies \hat{\mathcal{M}}(t)$$

[Xu et al., EAAI, 2025]

Reduced coordinates carry temporal dynamics

Learning F_θ reveals an intrinsic forecast map

$X(t) \in \mathbb{R}^{N_h}$ $\xrightarrow{\textbf{SVD}}$ $X(t) \simeq U_k\, a(t)$

HPR1000 xenon trajectory

$$a(t) = U_k^\top X(t), \qquad a(t) \in \mathbb{R}^k$$

GEIM / ST-GEIM

$$y_i = \ell_i(u) \implies c_j, \gamma_j$$

$$\hat{u}(x,t) = \sum_j \gamma_j \psi_j(x,t)$$

learned reduced flow

$$\widehat{a}(t+T) = \mathcal{F}_\theta(a(t), a(t-\Delta t), \ldots, a(t-L\Delta t))$$

GRU--LSTM

$$\widehat{X}(t+T) = U_k\, \widehat{a}(t+T)$$

future-field reconstruction

$\mathcal{M} \subset \mathbb{R}^{N_h}, \qquad a(t), \qquad \mathcal{F}_\theta \qquad \implies$ **reduced coordinates retain temporal dynamics**

[Gong et al., NSE, 2025]

Xenon memory in reduced coordinates

Long-horizon prediction validates the learned reduced flow

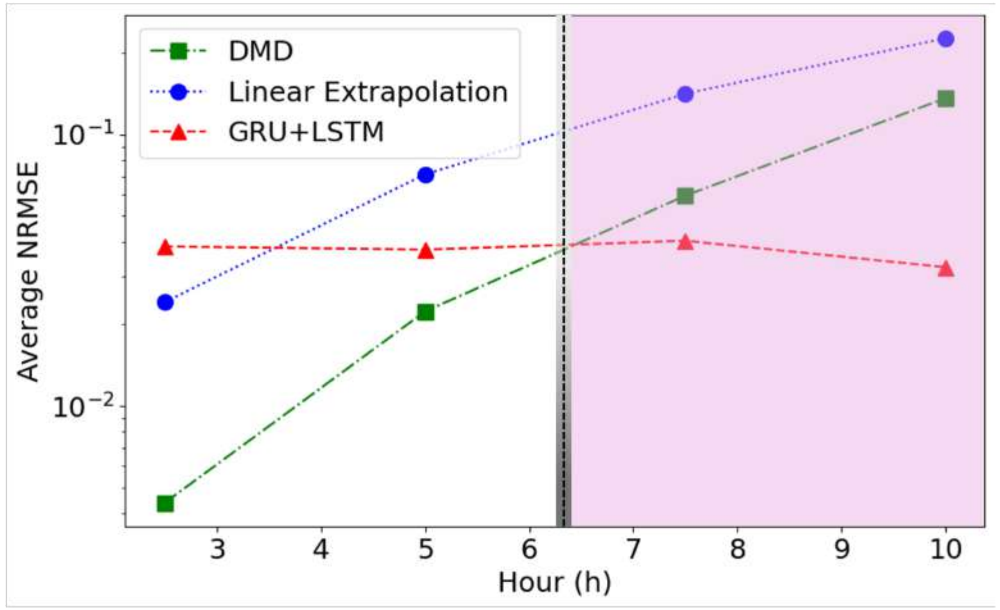

The forecast map learned in reduced coordinates remains stable as the horizon increases.

Power peak factor F_Q with input steps of 4h and a prediction horizon of 10h.

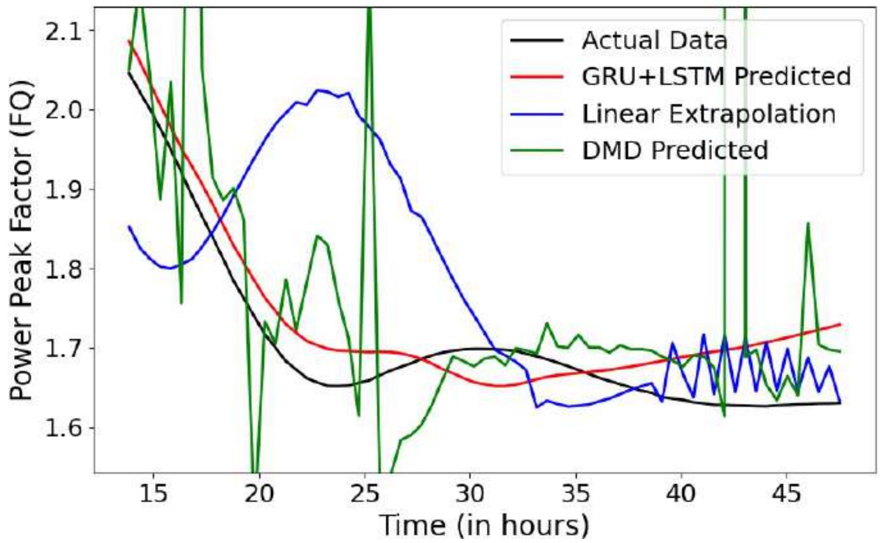

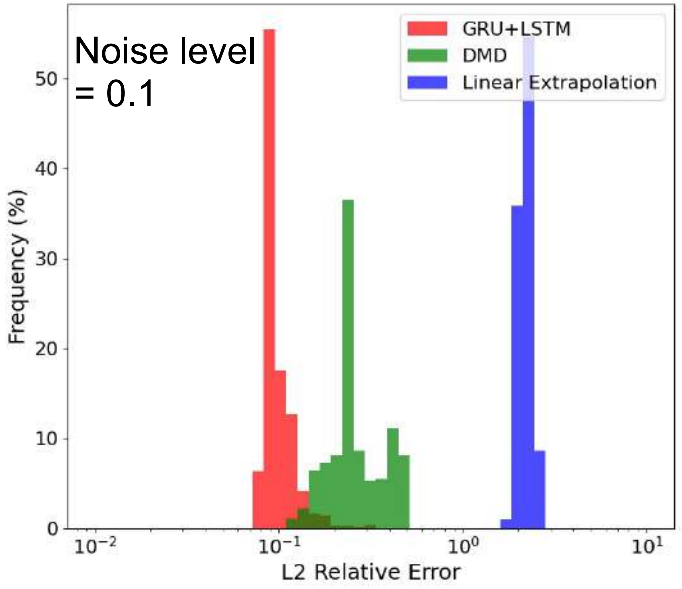

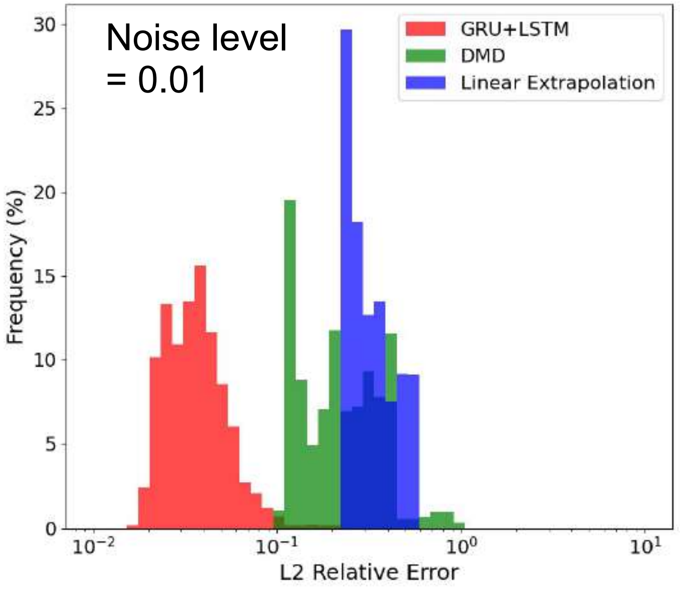

Reduced dynamics remain identifiable under noisy trajectories.

Comparison of model performance metrics for 30%FP with prediction horizon = 10 h

	L_2 relative error	R^2
SVD-GRU-LSTM	**0.0286**	**0.989**
DMD	0.0932	0.906
Linear	0.2450	0.428

[Gong et al., NSE, 2025]

Latent coupling infers unobserved fields

Sparse histories predict future power, xenon and iodine

Past input $x_{t-t_1:t}$ $\longrightarrow$ SHPNet latent neural operator Φ $\longrightarrow$ **Future output** $\{y^{rec}, z^{rec}, q^{rec}\}_{t+1:t+t_2}$

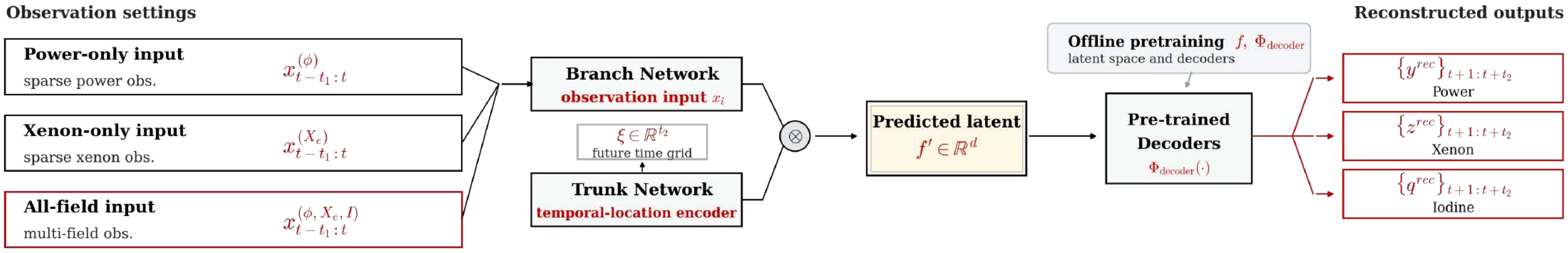

$x_{t-t_1:t} \to \{y^{rec}, z^{rec}, q^{rec}\}_{t+1:t+t_2}$ with $t_1 = 8\,\text{h}$, $t_2 = 15\,\text{h}$ in the result panel.

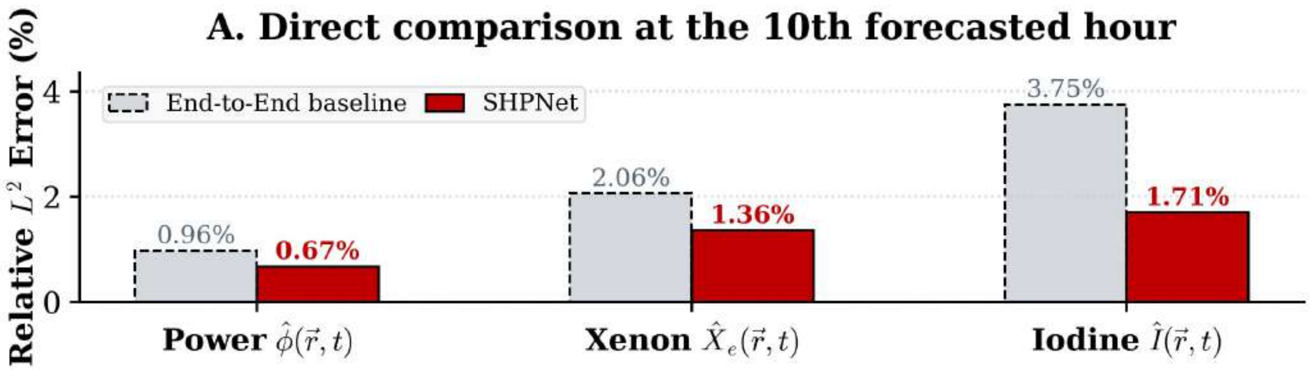

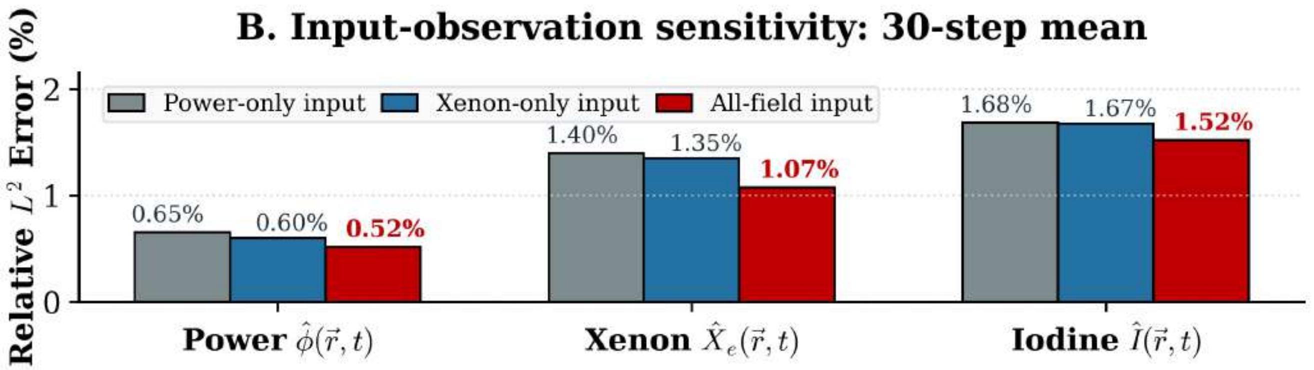

Temporal setting from the manuscript: 8 h historical observations $\rightarrow$ 15 h forecast (30 steps, $\Delta t = 0.5$ h).

[Xu et al., EAAI, 2025]

Space-time GEIM formulation (1/2)

State interpolation becomes trajectory reconstruction

From states to trajectories

$$\mathcal{M}_s = \{u(\cdot, t_k; \mu) : \mu \in \mathcal{D}\} \subset X(\Omega)$$

$$\mathcal{I}_M[u](x, t_k) \approx \sum_{j=1}^{M} \alpha_j(t_k, \mu)\, \varphi_j(x)$$

$\Longrightarrow$ **space-time generalization**

$$\mathcal{M}_{st} = \{u(\cdot, \cdot; \mu) : \mu \in \mathcal{D}\} \subset \mathcal{X}_{st}$$

$$y_k = \ell_k^{st}(u) = \sigma_k(u(\cdot, o_k, \mu)), \qquad \sigma_k \in \Sigma,\ o_k \in [0, t_k]$$

$\Longrightarrow$ **operator shift**

$$\mathcal{I}_M[u(\cdot, t_k)]_{\text{state}} \longrightarrow \mathcal{I}_{M_{st}}[u(\cdot, \cdot)]_{\text{trajectory}}$$

$$\hat{u}(x, t; \mu^{\text{true}}) \approx \sum_{j=1}^{M_{st}} \gamma_j(\mu^{\text{true}})\, \psi_j(x, t), \qquad \psi_j \in \mathcal{X}_{st}$$

spatiotemporal basis $\psi_j(x, t)$ and coefficients γ_j drive future-trajectory reconstruction

[Bao et al., JCP, 2025]

Space-time GEIM formulation (2/2)

State interpolation becomes trajectory reconstruction

Predictive mechanisms

(1) **STD-GEIM**

$$\hat{u}(x, t_{k+j}; \mu^{\text{true}}) = \sum_{m=1}^{M_s} \alpha_m(t_{k+j}, \mu^{\text{true}})\, \varphi_m(x)$$

$$B\boldsymbol{\alpha} = \boldsymbol{z}_{t_{k+j}}^{\text{predict}}$$

fixed spatial basis and fixed sensor locations
future sensor values are extrapolated first

(2) **EDMD-STD-GEIM**

$$\boldsymbol{\eta}_{k+j} = \mathbf{K}^j \Psi(\boldsymbol{z}_{t_k})$$

$$\boldsymbol{z}_{t_{k+j}}^{\text{predict}} = \mathbf{C}\boldsymbol{\eta}_{k+j} \implies B\boldsymbol{\alpha} = \boldsymbol{z}_{t_{k+j}}^{\text{predict}}$$

Koopman evolution acts on the observation vector
STD-GEIM then reconstructs the field

fully coupled space-time extension

(3) **STC-GEIM**

$$\mathcal{I}_{M_{st}}[u] = \sum_{i=1}^{M_{st}} \gamma_i(\mu)\, \psi_i(x, t)$$

$$\sum_{i=1}^{M_{st}} \gamma_i C_{k,i} = \sigma_k(u(\cdot, o_k, \mu))$$

space and time are encoded together in $\psi_i(x,t)$
and in $C_{k,i} = \sigma_k(\psi_i(\cdot, o_k))$

(4) **STC-LS-GEIM**

$$\hat{\gamma} = \arg\min_{\gamma \in \mathbb{R}^{M_{st}}} \|\boldsymbol{y} - \hat{C}\gamma\|_2^2$$

$$\hat{C} \in \mathbb{R}^{M_{st}^2 \times M_{st}}$$

overdetermined least-squares update with redundant observations
regularization can be added for noisy data

[Bao et al., JCP, 2025]

Single-Physics Forecasting

Goal

Consider a time interval $\mathcal{I} = [0, t_f]$ with discretization $0 = t_0 < t_1 < \cdots < t_k < \cdots < t_K = t_f$. Given the current time $t = t_k$, we aim to predict the true field $u(t, \mu^{\text{true}})$ at a future time $t = t_{k+j}$.

[Bao et al., JCP, 2025]

Method I: Spatiotemporal Decoupling GEIM

Variable separation meets temporal extrapolation

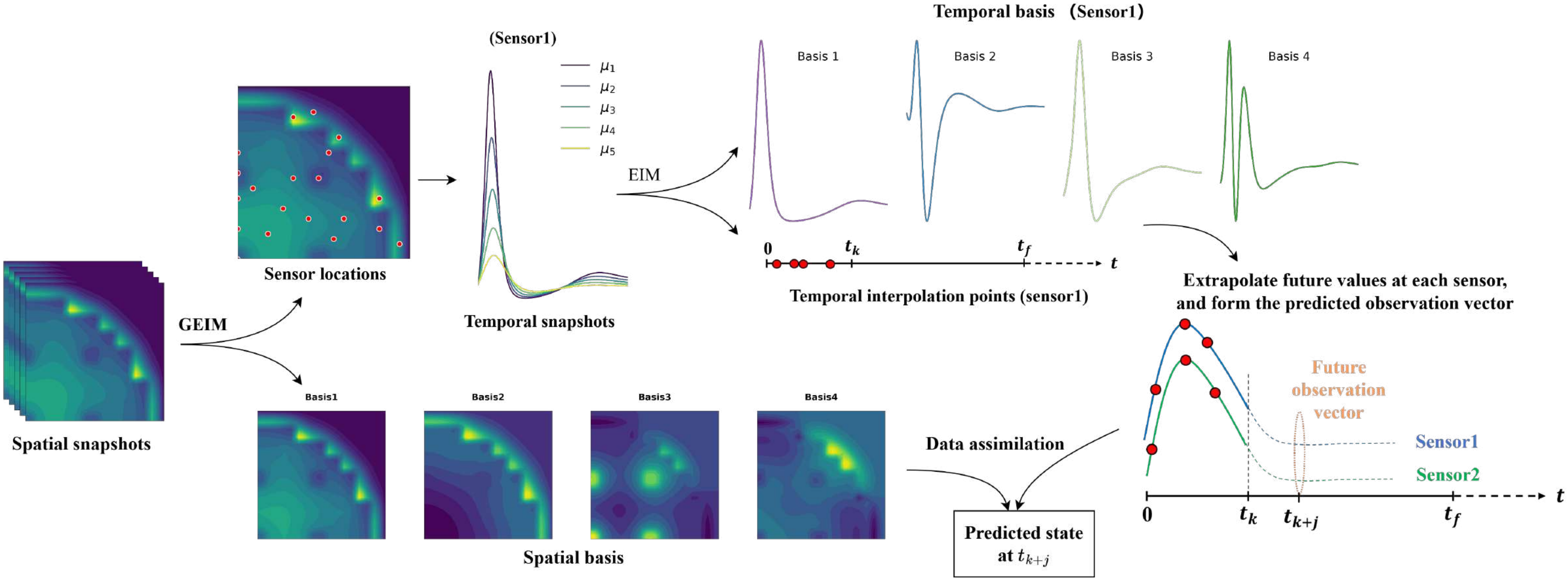

[Bao et al., JCP, 2025]

Method I: Spatiotemporal Decoupling GEIM

STD-GEIM Step 1& 2: Construct Basis

1. **Construct Spatial Basis:** Apply GEIM to spatial snapshots

$$\mathcal{S}_{\mathcal{M}} = \{u(t,\mu) : t \in \{t_1, \ldots, t_K\}, \mu \in \Xi_{\text{train}}\}$$

to get spatial basis $\{\varphi_m\}_{m=1}^{M}$ and spatial linear functionals $\{\sigma_m\}_{m=1}^{M}$.

2. **Construct Temporal Basis:** For *each* spatial linear functional σ_i:
   - Collect its time-series data:

$$\zeta^{(i)} = \left\{(\sigma_i(u(t_1,\mu)), \ldots, \sigma_i(u(t_K,\mu))) \,\middle|\, \mu \in \Xi_{\text{train}}\right\}.$$

   - Apply EIM to $\zeta^{(i)}$ to get the local temporal basis $\{q_l^{(i)}(t)\}_{l=1}^{M}$ and temporal interpolation points $\{\tau_l^{(i)}\}_{l=1}^{M} \subset [0, t_k]$.

[Bao et al., JCP, 2025]

Method I: Spatiotemporal Decoupling GEIM

STD-GEIM Step 3: Temporal extrapolation

3. Forecast Future Sensor Values (for each sensor σ_i):

- For $u(t, \mu^{\text{true}})$, collect past observations $\boldsymbol{y}_{obs}^{(i)}$ at times $\{\tau_l^{(i)}\}_{l=1}^M$.
- Reconstruct the local time series by finding coefficients $\boldsymbol{\beta}^{(i)}$ in:

$$\sigma_i(u(t, \mu^{\text{true}})) \approx \sum_{l=1}^{M} \beta_l^{(i)} \boldsymbol{q}_l^{(i)}(t)$$

$$\underbrace{\sigma_i(u(\tau_j^{(i)}, \mu^{\text{true}}))}_{\boldsymbol{y}_{obs}^{(i)}} = \sum_{l=1}^{M} \beta_l^{(i)} \boldsymbol{q}_l^{(i)}(\tau_j^{(i)}), \quad j = 1, \cdots, M.$$

- Obtain measurements at t_{k+j}.

[Bao et al., JCP, 2025]

Method I: Spatiotemporal Decoupling GEIM

STD-GEIM Step 4: Reconstruct

4. Reconstruct field at t_{k+j}:

- Form predicted observation vector $\boldsymbol{z}_{t_{k+j}}^{\text{pred}}$.
- Reconstruct field at t_{k+j} by finding coefficients $\alpha_m(t_{k+j})$ in:

$$u(t_{k+j}, \mu^{\text{true}}) \approx \sum_{m=1}^{M} \alpha_m(t_{k+j}, \mu^{\text{true}}) \varphi_m(x)$$

$$\left(\boldsymbol{z}_{t_{k+j}}^{\text{pred}}\right)_i = \sum_{m=1}^{M} \alpha_m(t_{k+j}, \mu^{\text{true}}) \sigma_i(\varphi_m), \quad i = 1, \cdots, M.$$

[Bao et al., JCP, 2025]

Method II: Extended Dynamic Mode Decomposition STD-GEIM

Incorporate DMD technique into STD-GEIM

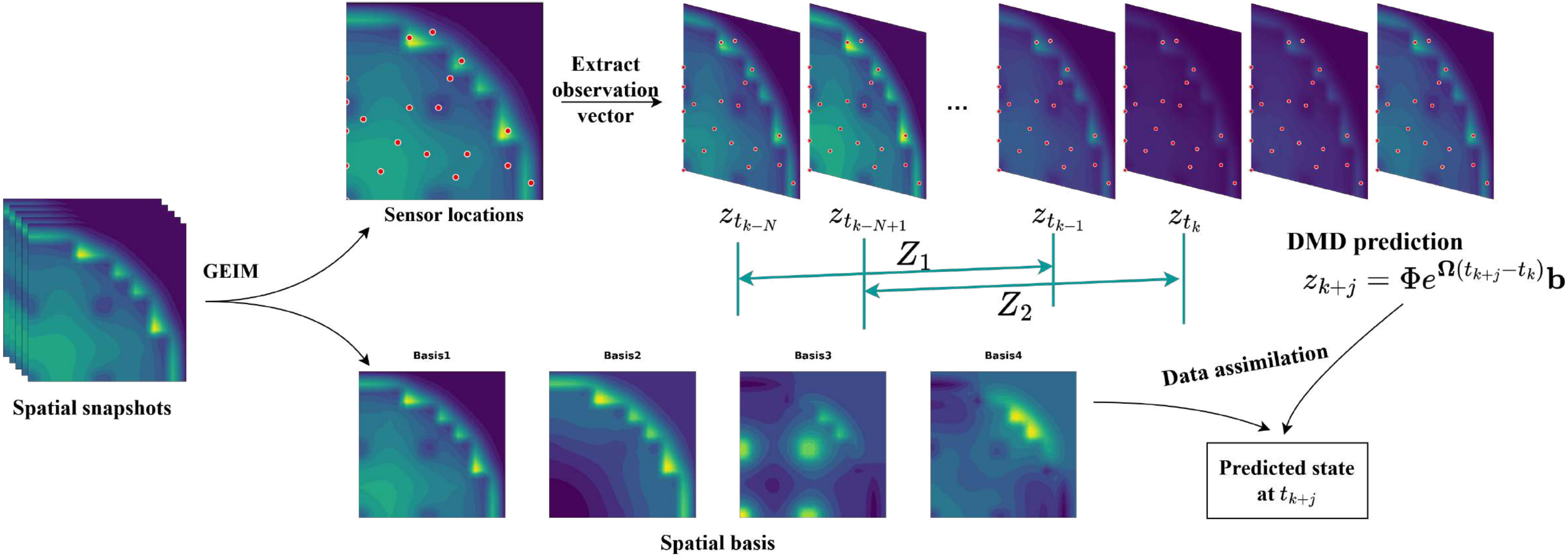

[Bao et al., JCP, 2025]

Method II: Extended Dynamic Mode Decomposition STD-GEIM

Incorporate DMD technique into STD-GEIM

Workflow:

1. **Build Basis:** Apply GEIM to spatial snapshots to get spatial basis $\{\varphi_m\}_{m=1}^M$ and functionals $\{\sigma_m\}_{m=1}^M$.
2. **Collect History:** Gather observation vector sequence $\{\boldsymbol{z}_{k-N}, \ldots, \boldsymbol{z}_k\}$.
3. **Forecast:** Employ EDMD on the sequence $\{\boldsymbol{z}_i\}$ to learn a linear operator and predict future observation vector $\boldsymbol{z}_{t_{k+j}}^{\mathrm{pred}}$.
4. **Reconstruct:** Solve the linear system and reconstruct the field

$$\left(\boldsymbol{z}_{t_{k+j}}^{\mathrm{pred}}\right)_i = \sum_{m=1}^{M} \alpha_m(t_{k+j})\sigma_i(\varphi_m), \quad i = 1, \cdots, M.$$

[Bao et al., JCP, 2025]

Method III: Spatiotemporal Coupling GEIM

Construct a spatiotemporal low-dimensional subspace

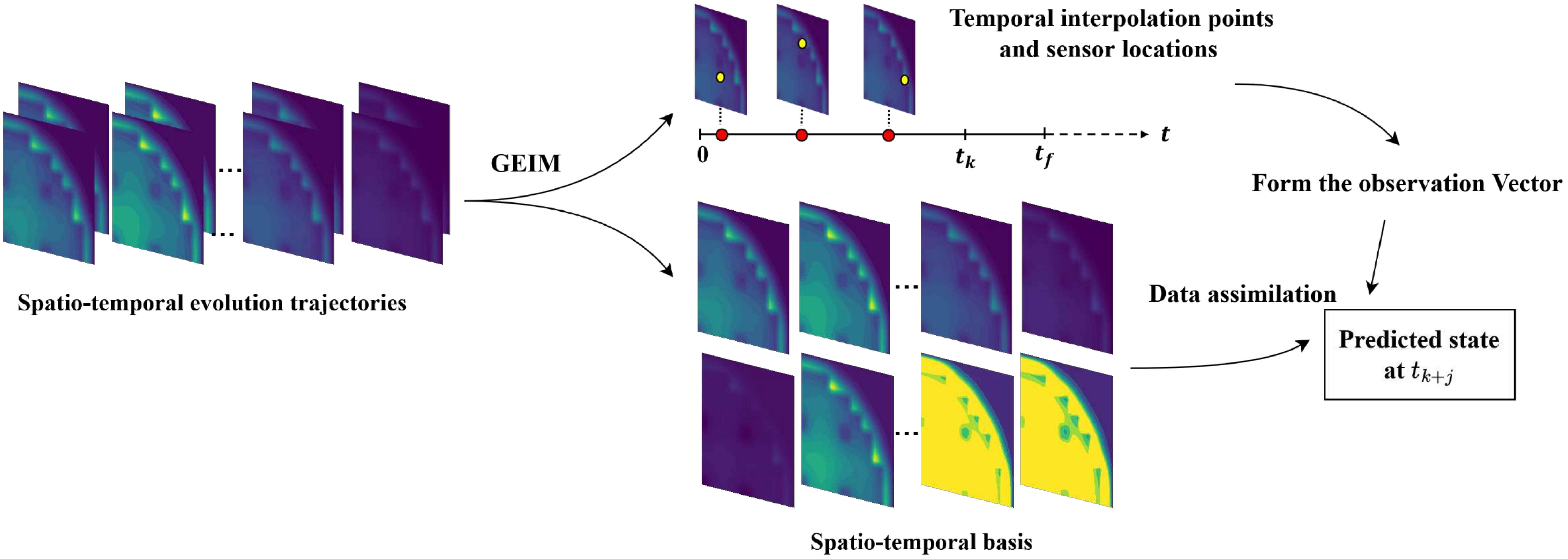

[Bao et al., JCP, 2025]

Method III: Spatiotemporal Coupling GEIM

Construct a spatiotemporal low-dimensional subspace

Core Idea

- Let $\Omega := \mathcal{R} \times [0, t_f] \subset \mathbb{R}^d \times \mathbb{R}$ and $\mathcal{X}_{st}$ be a Banach space on Ω.
- Assume the solution manifold $\mathcal{M}_{st} := \{u(\cdot, \cdot, \mu) \in \mathcal{X}_{st} \,|\, \mu \in \mathcal{D}\}$ is compact in $\mathcal{X}_{st}$.
- **Goal:** Construct a spatiotemporal low-dimensional subspace $X^{st}_{M_{st}} \subset \mathcal{X}_{st}$ with $M \ll \dim(\mathcal{M}_{st})$ such that for any $u \in \mathcal{M}_{st}$

$$u(x, t, \mu) \approx \sum_{i=1}^{M} \alpha_i(\mu)\psi_i(x, t),$$

where $\{\psi_i(x, t)\}_{i=1}^{M}$ are **spatiotemporal basis** extracted by a greedy procedure very similar to GEIM.

[Bao et al., JCP, 2025]

GEIM

Input: $\{u(\mu)\}_{\mu\in\Xi_{\text{train}}}$, Σ, ε_{tol}
Output: $\{\varphi_i\}$, $\{\sigma_i\}$

First iteration:
$\mu_1 = \arg\max_\mu \|u(\mu)\|_{\mathcal{X}}$
$\sigma_1 = \arg\max_\sigma |\sigma(u(\mu_1))|$
$\varphi_1 = u(\mu_1)/\sigma_1(u(\mu_1))$

while $M < M_{\text{max}}$ **do**
  Interpolant: $\mathcal{I}_M[u](\mu) = \sum_{i=1}^M \beta_i(\mu)\varphi_i$
  $\sigma_j(u(\mu)) = \sigma_j(\mathcal{I}_M[u]),\ j = 1,\dots,M$
  Residual: $e_M(\mu) = u(\mu) - \mathcal{I}_M[u](\mu)$
  $\mu_{M+1} = \arg\max_\mu \|e_M(\mu)\|_{\mathcal{X}}$
  if $\|e_M(\mu_{M+1})\| < \varepsilon_{\text{tol}}$ **then**
    break
  end if
  $\sigma_{M+1} = \arg\max_\sigma |\sigma(e_M(\mu_{M+1}))|$
  $\varphi_{M+1} = e_M(\mu_{M+1})/\sigma_{M+1}(e_M(\mu_{M+1}))$
  $M \leftarrow M+1$
end while

STC-GEIM

Input: $\{u(t,\mu)\}_{\mu\in\Xi_{\text{train}}}$, Σ, ε_{tol}
Output: $\{\psi_i\}$, $\{\sigma_i\}$, $\{o_i\}$

First iteration:
$(\mu_1, o_1) = \arg\max_{\mu, t\in[0,t_k]} \|u(\cdot,t,\mu)\|$
$\sigma_1 = \arg\max_\sigma |\sigma(u(\cdot,o_1,\mu_1))|$
$\psi_1 = u(\cdot,\cdot,\mu_1)/\sigma_1(u(\cdot,o_1,\mu_1))$

while $M < M_{\text{max}}$ **do**
  Interp: $\mathcal{I}_M[u](t,\mu) = \sum_{i=1}^M \gamma_i(\mu)\psi_i(x,t)$
  $\sigma_j(u(\cdot,o_j,\mu)) = \sigma_j(\mathcal{I}_M[u](o_j)),\ j = 1,\cdots,M$
  Residual: $e_M(t,\mu) = u(t,\mu) - \mathcal{I}_M[u](t,\mu)$
  $(\mu_{M+1}, o_{M+1}) = \arg\max_{\mu,t\in[0,t_k]} \|e_M(t,\mu)\|$
  if $\|e_M(o_{M+1},\mu_{M+1})\| < \varepsilon_{\text{tol}}$ **then**
    break
  end if
  $\sigma_{M+1} = \arg\max_\sigma |\sigma(e_M(o_{M+1},\mu_{M+1}))|$
  $\psi_{M+1} = e_M(t,\mu_{M+1})/\sigma_{M+1}(e_M(o_{M+1},\mu_{M+1}))$
  $M \leftarrow M+1$
end while

Method III: Spatiotemporal Coupling GEIM

Forecasting Stage

- $X_{M_{st}}^{st} = \text{span}\{\psi_i\}_{i=1}^{M}$, any $u \in \mathcal{M}_{st}$ can be approximated by

$$u(x, t, \mu) \approx \sum_{i=1}^{M} \gamma_i(\mu)\, \psi_i(x, t).$$

- To determine the coefficients $\{\gamma_i(\mu)\}_{i=1}^{M}$, we collect observations from sensor σ_j at time point o_j, form an **observation vector** and then solve the linear system:

$$\sum_{i=1}^{M} \gamma_i(\mu)\, C_{j,i} = \sigma_j(u(\cdot, o_j, \mu)), \quad j = 1, \ldots, M,$$

where $C_{j,i} = \sigma_j(\psi_i(\cdot, o_j))$.

- The **prediction of** $u(x, t, \mu^{\mathrm{true}})$ **at time** t_{k+j} can be approximated by

$$u(x, t_{k+j}, \mu^{\mathrm{true}}) \approx \mathcal{I}_{M+1}[u](x, t_{k+j}, \mu^{\mathrm{true}}).$$

[Bao et al., JCP, 2025]

Method IV: Spatiotemporal Coupling Least-Squares GEIM

Combine STC-GEIM with least squares methods

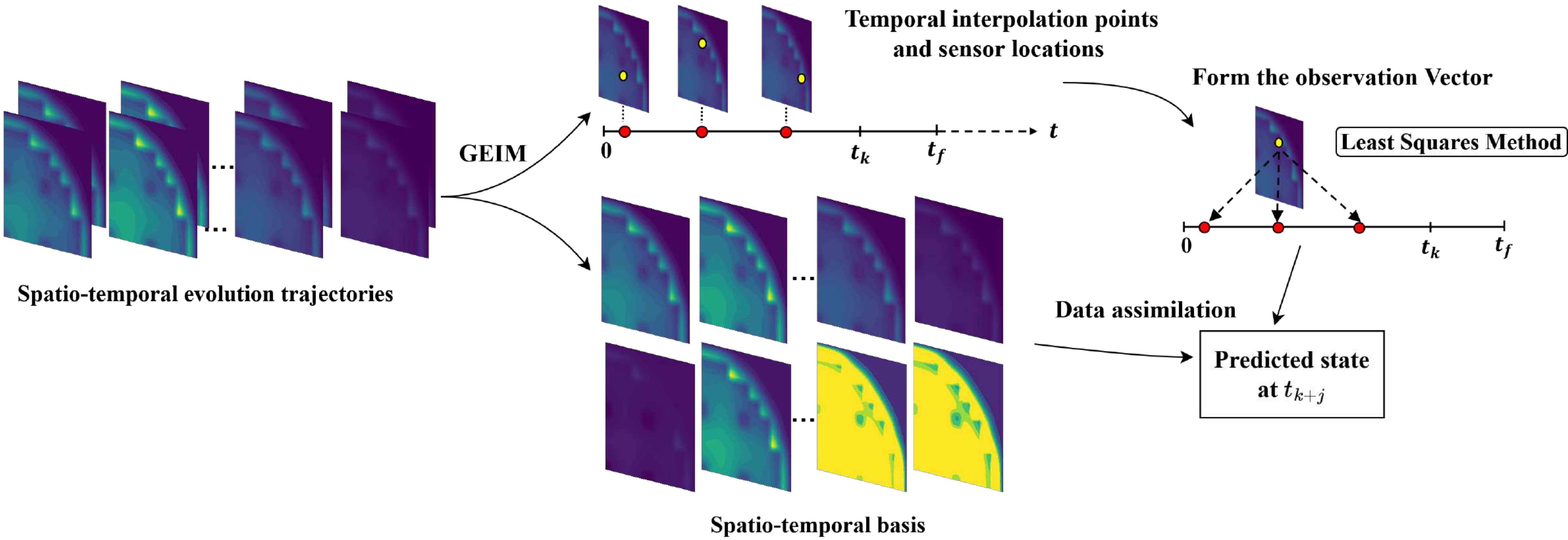

[Bao et al., JCP, 2025]

Method IV: Spatiotemporal Coupling Least-Squares GEIM

Combine STC-GEIM with least squares methods

- In **STC-GEIM**, each sensor σ_k is associated with a unique time point o_k.
- In **STC-LS-GEIM**, at each sensor location σ_i, we collect measurements at **all** M time points $\{o_j\}_{j=1}^{M}$, forming a larger observation set:

$$\{y_{ij} = \sigma_i(u(\cdot, o_j, \mu^{\text{true}}))\}_{i,j=1}^{M}.$$

- We then solve the following **least-squares problem** to obtain the coefficients:

$$\hat{\gamma} = \arg\min_{\gamma \in \mathbb{R}^M} \sum_{j=1}^{M} \sum_{i=1}^{M} \Big| y_{ij} - \underbrace{\sum_{k=1}^{M} \gamma_k \sigma_i(\psi_k(\cdot, o_j))}_{\text{Approx.}} \Big|^2.$$

[Bao et al., JCP, 2025]

Multi-Physics Forecasting

The Challenge

To simultaneously predict the future states of four coupled physical fields (ϕ_1, ϕ_2, P, T) using observations of ϕ_2 only.

[Bao et al., JCP, 2025]

The Challenge

To simultaneously predict the future states of four coupled physical fields (ϕ_1, ϕ_2, P, T) using observations of ϕ_2 only.

Single-Physics Forecasting

- STD-GEIM
- STC-GEIM
- STC-LS-GEIM
- EDMD-STD-GEIM

Vectorial Extension

Multi-Physics Forecasting

- MP STD-GEIM
- MP STC-GEIM
- MP STC-LS-GEIM
- MP EDMD-STD-GEIM

[Bao et al., JCP, 2025]

The Challenge

To simultaneously predict the future states of four coupled physical fields (ϕ_1, ϕ_2, P, T) using observations of ϕ_2 only.

Solution: Vectorial Extension of GEIM

1. Treat (ϕ_1, ϕ_2, P, T) as a vector field.
2. Build basis functions for all four fields but **share the coefficients**.
3. Select sensor locations based on the observable field ϕ_2.
4. Use ϕ_2 measurements to determine the coefficients.

$$\mathbf{U}(x, t; \mu) = [\phi_1, \phi_2, P, T]^\top (x, t; \mu)$$

$$\mathbf{U}(x, t; \mu) \approx \sum_{m=1}^{M_s} \alpha_m(t, \mu) \left[\varphi_m^1, \varphi_m^2, \varphi_m^P, \varphi_m^T\right]^\top .$$

Numerical Results for the IAEA 2D PWR Problem

The temperature field differs significantly in spatial distribution and evolves with a temporal lag compared to the other physical fields.

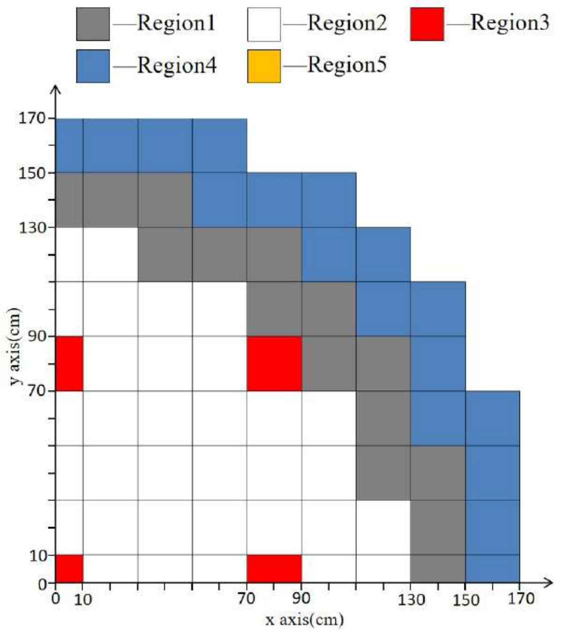

- **Two-Group Neutron Kinetics (with Precursor Feedback):**

$$\frac{1}{v_1}\frac{\partial \phi_1}{\partial t} = \nabla \cdot D_1(T)\nabla\phi_1 - \Sigma_{r1}(T)\phi_1 + \frac{1-\beta}{k_{\text{eff}}}\sum_{g=1}^{2}\nu\Sigma_{fg}\phi_g + \lambda C$$

$$\frac{1}{v_2}\frac{\partial \phi_2}{\partial t} = \nabla \cdot D_2(T)\nabla\phi_2 - \Sigma_{a2}(T)\phi_2 + \Sigma_{s,1\to 2}\phi_1$$

- **Power Generation & Thermal-Hydraulics Heat Equation:**

$$P(\vec{r},t) = \kappa\sum_{g=1}^{2}\Sigma_{fg}\phi_g$$

$$\rho c_p\frac{\partial T}{\partial t} = \nabla \cdot K\nabla T + P(\vec{r},t) - q_{\text{cool}}(T)$$

Cross-Field Parameter Feedback (Doppler & Moderator Effects):

$$T(\vec{r},t) \;\Rightarrow\; \Sigma_{a,g}(T) = \Sigma_{a,g}^{0} + \gamma_a\sqrt{T}, \quad D_g(T) = D_g^0 + \gamma_D T$$

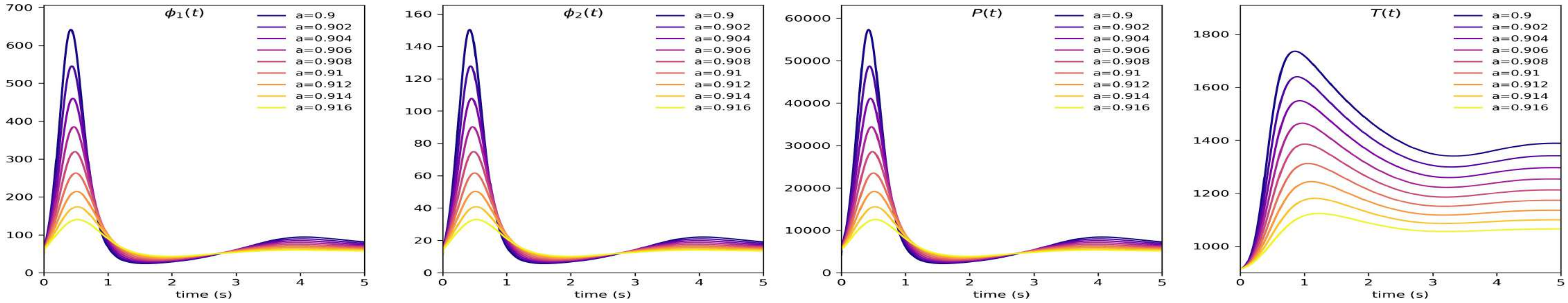

Evolution of four fields at spatial point (30, 30) over time.

[Bao et al., JCP, 2025]

Single-Physics Forecasting: Long-Term Prediction

Numerical Results for the IAEA 2D PWR Problem

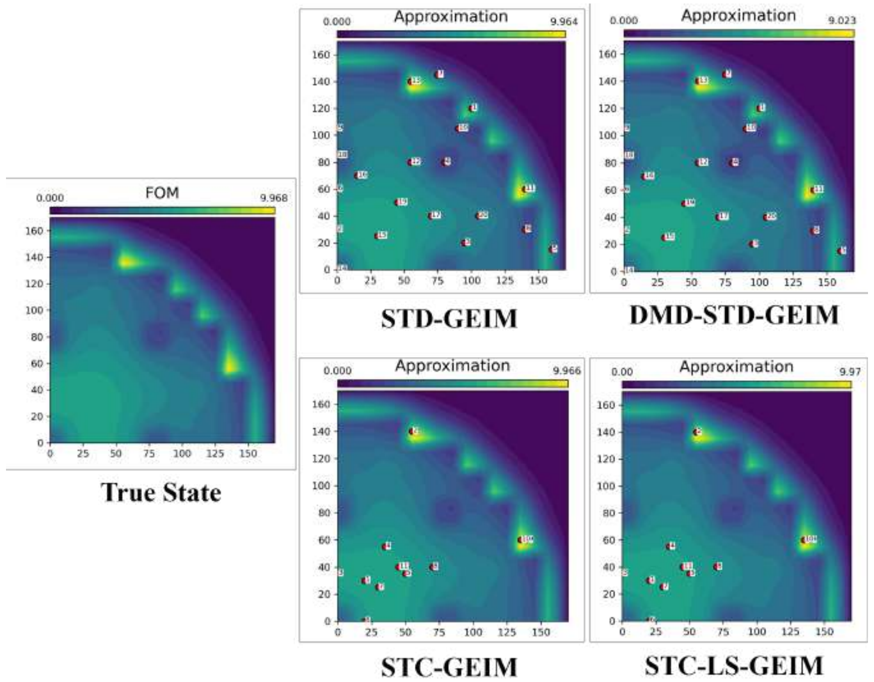

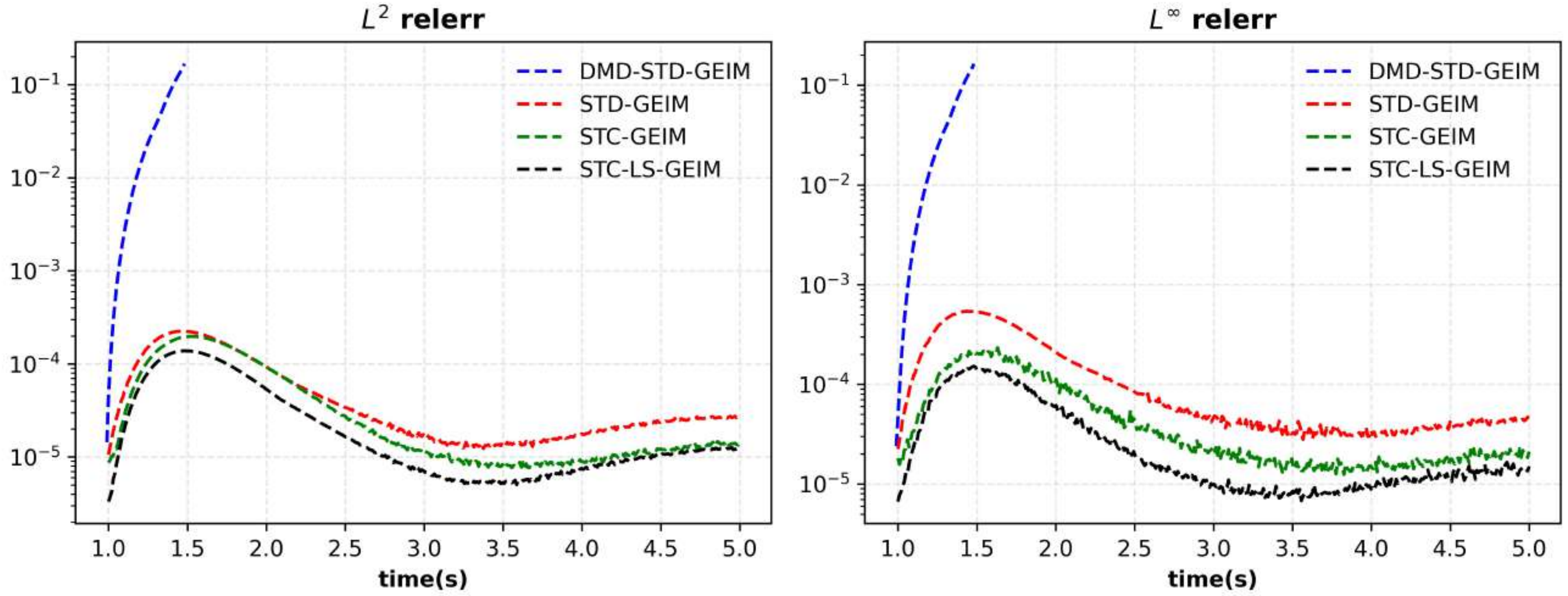

Goal: Predict ϕ_2 from $t_k = 1.0s$ and show the evolution of error over time.

Conclusion:

- EDMD-STD-GEIM (operator-based) is effective for **short-term** prediction.
- The spatiotemporal coupled methods (STC-GEIM, STC-LS-GEIM) consistently outperform the decoupled approach (STD-GEIM).

[Bao et al., JCP, 2025]

Single-Physics Forecasting with Noisy Observations

Numerical Results for the IAEA 2D PWR Problem

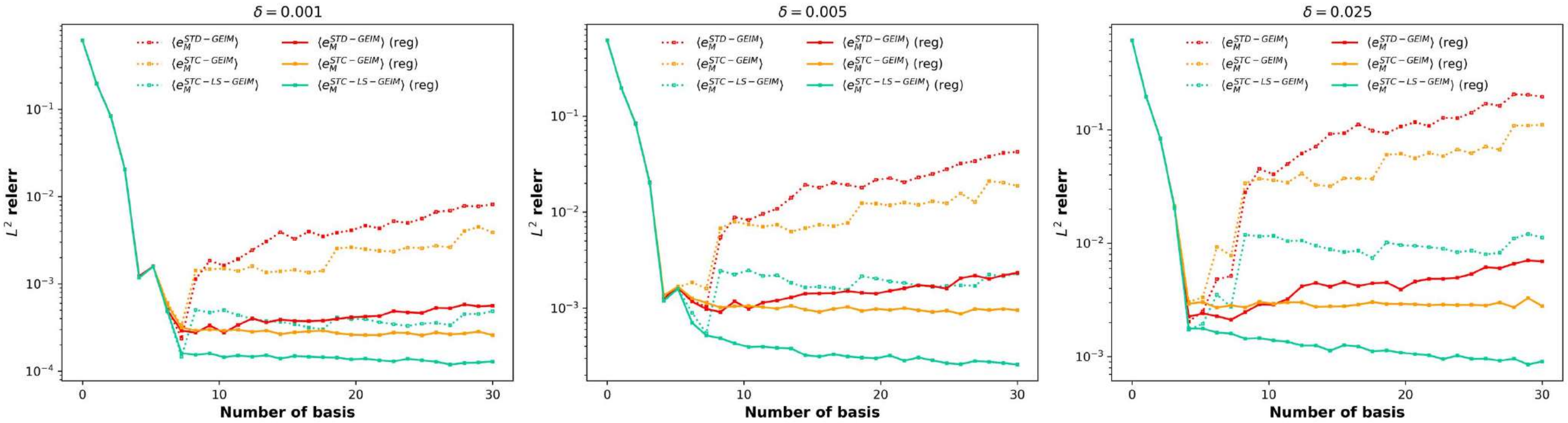

Goal: Assess the impact of observation noise on prediction accuracy and the effectiveness of **Tikhonov regularization** in reducing error growth.

Conclusion:

- Regularization is crucial for stability.
- STC-LS-GEIM is exceptionally robust, maintaining low error and stable convergence even with significant noise.

[Bao et al., JCP, 2025]

Multi-Physics Forecasting (observe Φ_2)

Numerical Results for the IAEA 2D PWR Problem

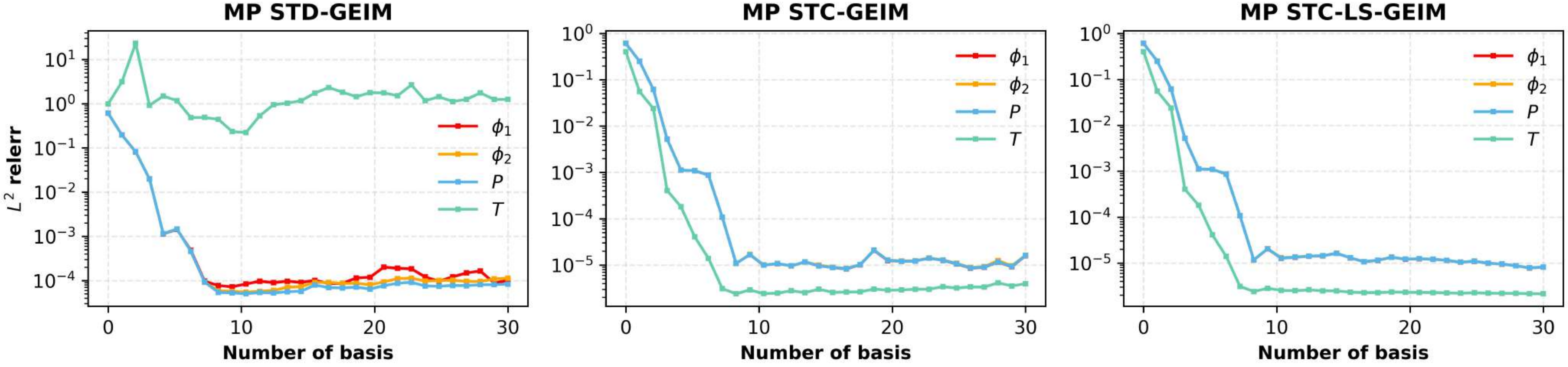

Conclusion:

- Due to the decoupled nature, MP STD-GEIM fails to capture the temporal lag in the temperature dynamics.
- The **spatiotemporal coupled methods** demonstrate strong performance even for fields with distinct evolutionary trajectories or spatial distributions.

[Bao et al., JCP, 2025]

Multi-Physics Forecasting (observe Φ_1, P or T)

Numerical Results for the IAEA 2D PWR Problem

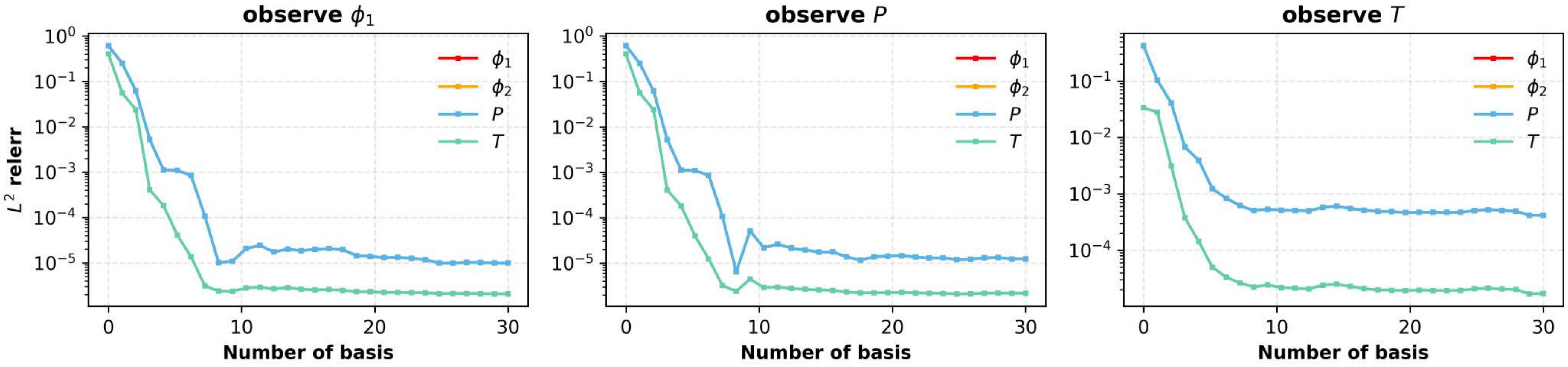

Conclusion: The spatiotemporal coupled methods consistently achieve high prediction accuracy across different observation scenarios.

[Bao et al., JCP, 2025]

Multi-Physics Forecasting: Long-Term Prediction

Numerical Results for the IAEA 2D PWR Problem

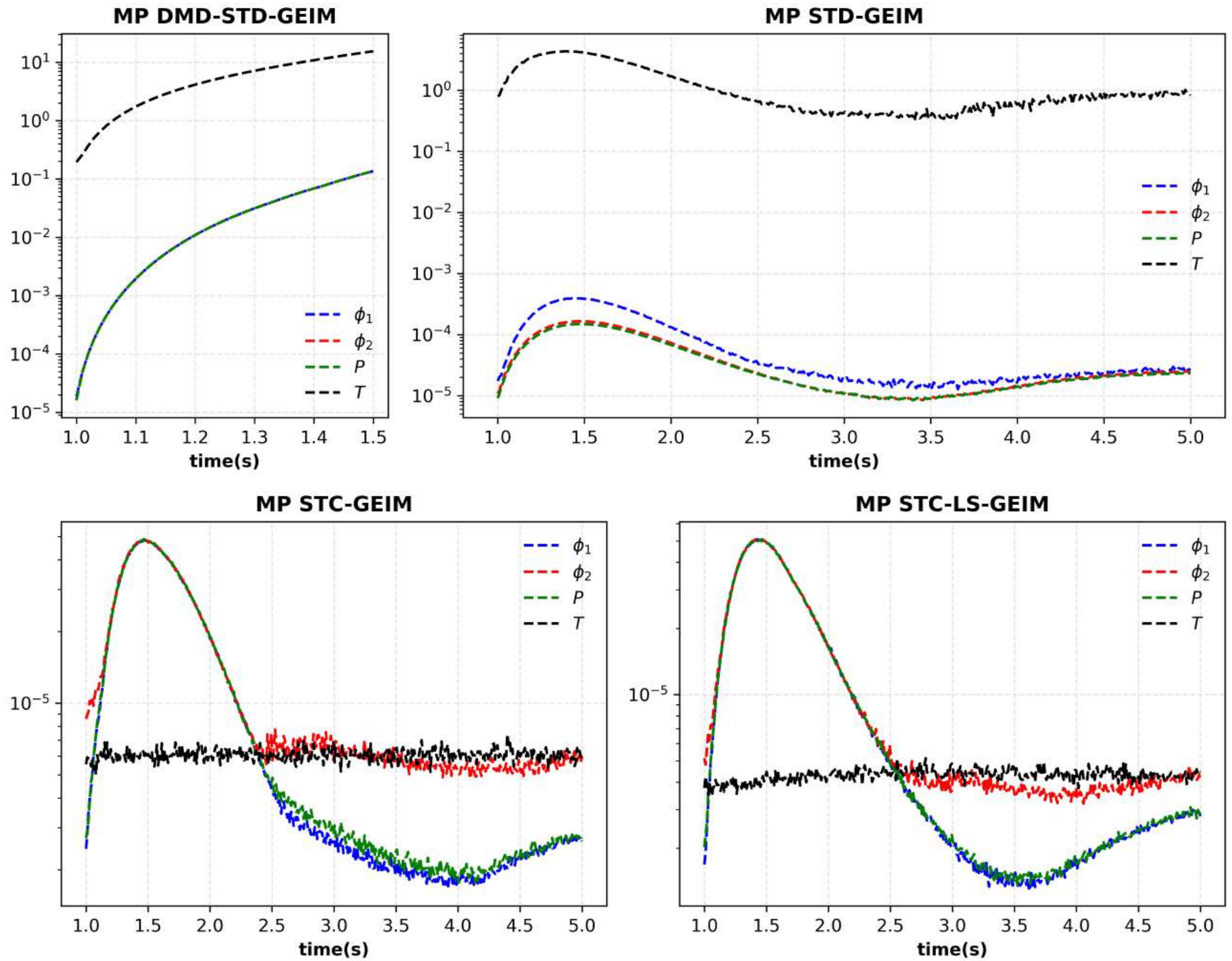

Conclusion: The long-term prediction capability of the spatiotemporal coupled methods supports **ultra-real-time forecasting**, providing operators with sufficient time to respond.

[Bao et al., JCP, 2025]

Test on reactor-scale : HPR1000 xenon oscillation

Long-term delayed coupling in 3D core dynamics

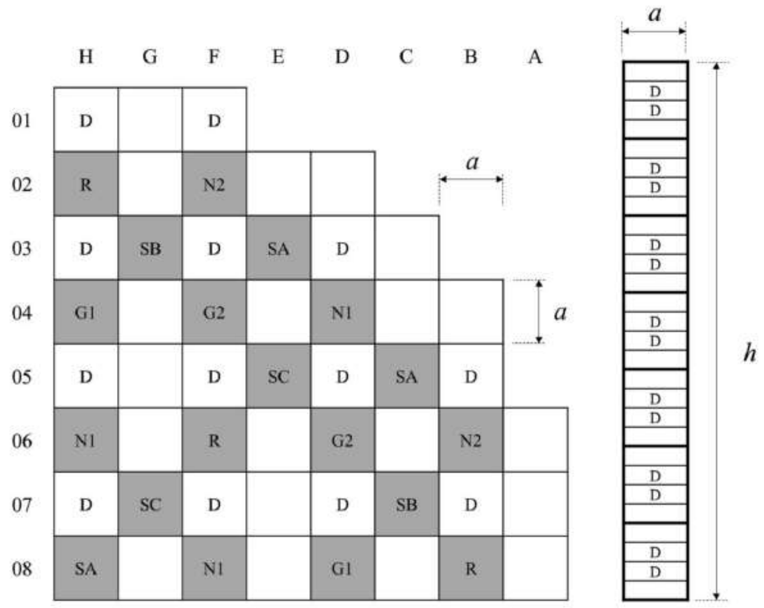

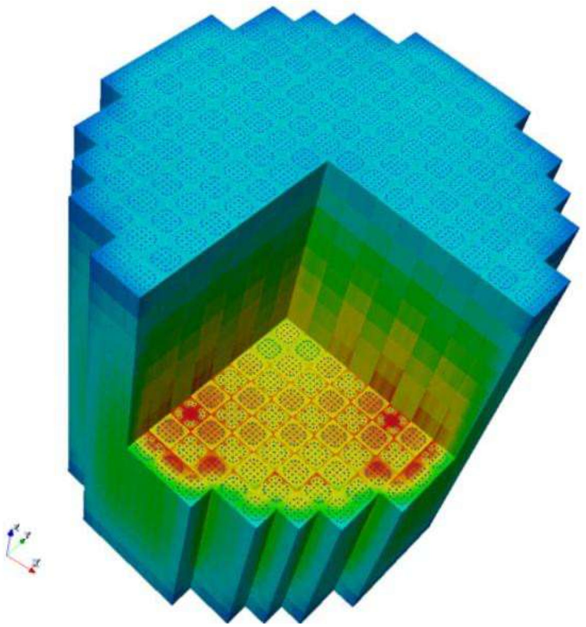

HPR1000 xenon oscillation

Governing Multiphysics System & Sparse Observation

Neutronics : $\frac{1}{v}\frac{\partial \phi}{\partial t} = \nabla \cdot (D\nabla\phi) + \left[(1-\beta)\nu\Sigma_f - \Sigma_a(T) - \sigma_a^X X_e(\phi)\right]\phi + \lambda C$

Thermal-Hydraulics : $\rho C_p \frac{\partial T}{\partial t} + \rho C_p \vec{u} \cdot \nabla T = \nabla \cdot (k\nabla T) + \kappa \Sigma_f \phi$

Isotope Poisoning : $\frac{\partial I}{\partial t} = \gamma_I \Sigma_f \phi - \lambda_I I, \quad \frac{\partial X_e}{\partial t} = \gamma_X \Sigma_f \phi + \lambda_I I - (\lambda_X + \sigma_a^X \phi) X_e$

Sparse Observation : $\mathcal{Y}_{\text{obs}}(t) = \mathbf{C}_{\text{sparse}} \cdot \phi(\vec{r}_{\text{sensor}}, t) + \epsilon$

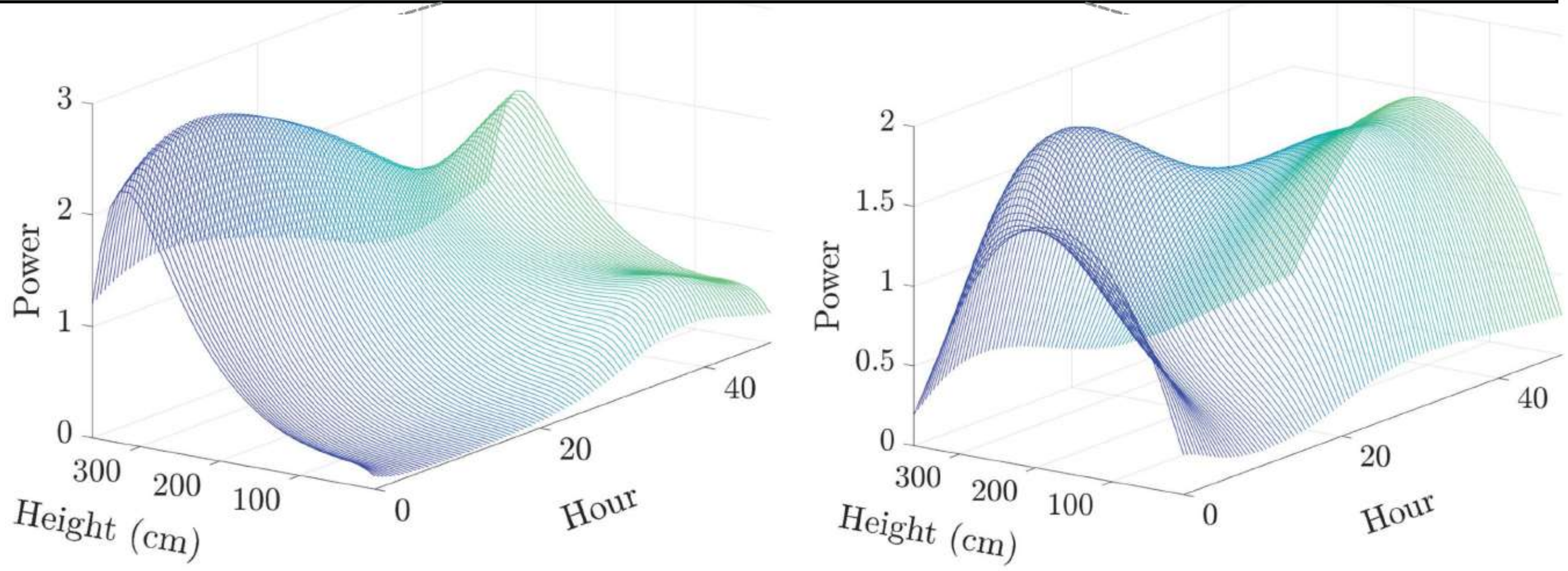

[Bao et al., JCP, 2025]

Ultra-real-time HPR1000 forecasting

Long-horizon multi-physics prediction with sub-second online update

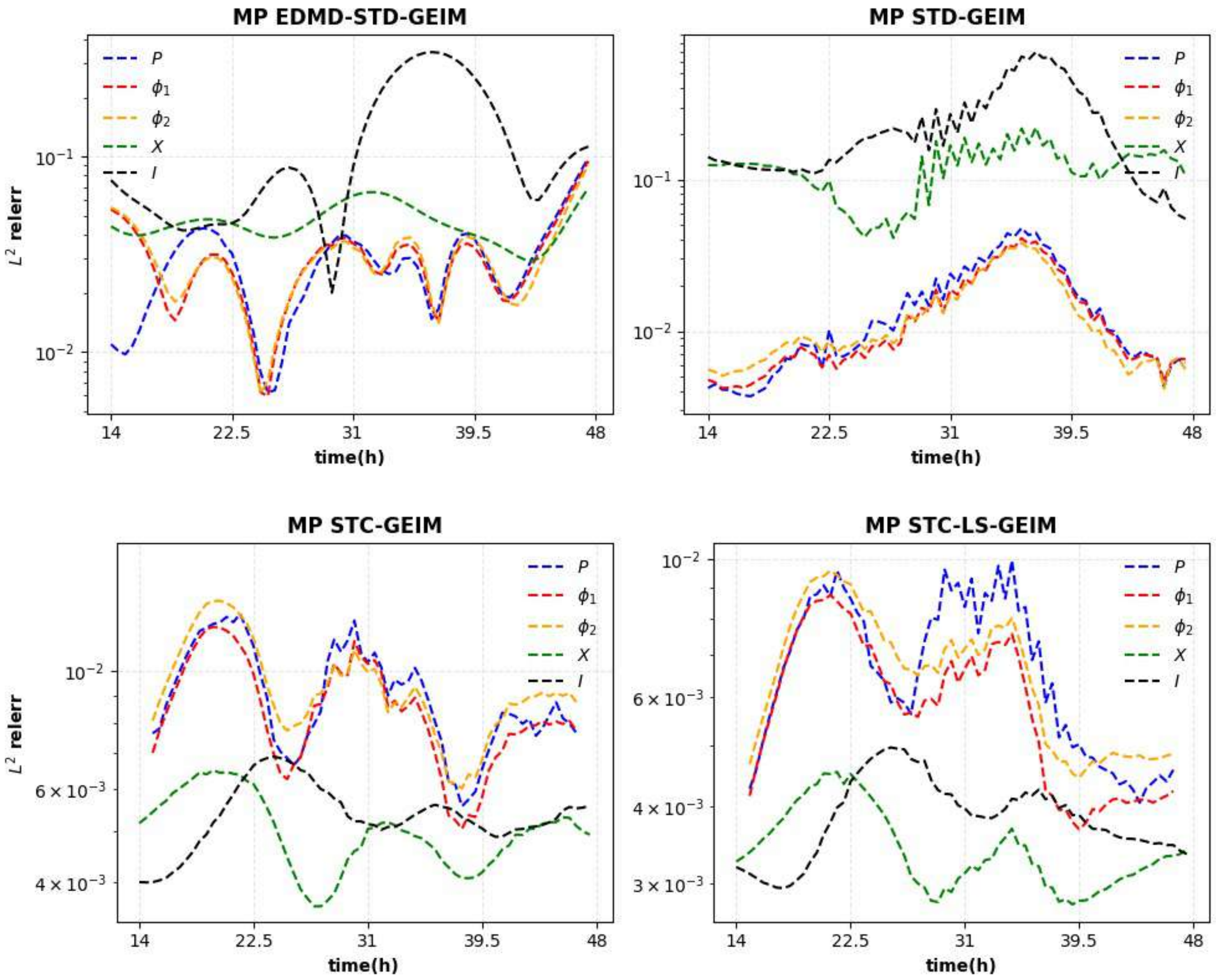

Offline: high-fidelity trajectories and bases. Online: reduced evaluation.

Online cost for multi-physics forecasting

Method	**Online time**
MP STD-GEIM	**0.134 s**
MP STC-GEIM	**0.158 s**
MP STC-LS-GEIM	**0.164 s**

$\mathcal{O}(10^{-1})\,\mathrm{s}$

online update

small linear systems
basis combination

Offline / online split

High-fidelity cost is offline; online prediction is sub-second.

[Bao et al., JCP, 2025]

From finite information to margin-informed operation

Complexity reduction turns sparse observations into credible reactor-state knowledge

Sparse observations		Stable reduced reconstruction		Parameter / state inference		Nonlinear reduced representation		Multi-field trajectory forecasting		Credible margin support
$\mathcal{Y}_{\text{obs}}, \mathcal{M}(\mathbf{u})$	$\Longrightarrow$	$\mathbf{u}_n \in \mathcal{X}_n$	$\Longrightarrow$	$\pi(\mu \mid y)$	$\Longrightarrow$	$\mathbf{z} \in \mathcal{Z}_{\text{latent}}$	$\Longrightarrow$	$\mathbf{u}(x, t_{>k})$	$\Longrightarrow$	Λ_{safe}

Sparse observations are progressively converted into future state knowledge and safety-margin support.

1. Finite information

Sparse measurements can still identify reactor states in reduced spaces.

2. Uncertainty reduction

Reduced inference decreases state, parameter, and multi-field uncertainty step by step.

3. Reduced dynamics

Low-dimensional coordinates retain nonlinear structure and temporal dynamics.

4. Operational value

Better online estimation supports margin assessment with less unnecessary conservatism.

For nuclear engineering, complexity reduction is valuable when it turns finite and imperfect information into credible safety-margin knowledge.

Thank you.

References

- Maday & Mula, Springer, 2013. Generalized empirical interpolation for reduced-basis data assimilation.
- Maday et al., IJNME, 2015. Parameterized-background data-weak variational data assimilation.
- Argaud et al., ICOSAHOM/Springer, 2017. Stabilization of (G)EIM under measurement noise.
- Argaud et al., JCP, 2018. Sensor placement in nuclear reactors based on GEIM.
- Gong et al., NED, 2020. Stabilized gappy POD for reactor power distribution estimation.
- Gong et al., NED, 2021. Fast field reconstruction with reduced basis and limited observations.
- Gong et al., Front. Energy Res., 2022. GEIM with H1 regularization for reactor physics.
- Gong et al., ANE, 2022. SVD autoencoder and generalized latent assimilation for reactor digital twins.
- Zeng et al., NST, 2023. Ensemble Bayesian inference for parameter distributions in reactor physics.
- Gong et al., NST, 2024. Reactor field reconstruction from sparse and movable sensors.
- Li et al., CiCP, 2024. Noise and vibration tolerant ResNet for sparse-sensor field reconstruction.
- Xu et al., NSE, 2025. Deep-learning-based reactor-core field reconstruction.
- Gong & Li, NSE, 2025. Reduced-order hybrid recurrent neural network for xenon dynamics.
- Xu et al., EAAI, 2025. Latent-coupled neural network for multi-physics forecasting.
- Bao et al., JCP, 2025. Spatiotemporal GEIM for ultra-real-time coupled multi-physics prediction.
- Zhang et al., NMTMA, 2025. Online updating criteria for reduced-order basis functions.
- Zheng et al., ANE, 2026. Spatiotemporal EIM for long-term xenon dynamics in commercial reactor cores.
- Li, Gong & Xu, CiCP, 2026. Neural-network-augmented EIM with noise and vibration tolerance.